



Controls on cave drip water temperature and implications for speleothem-based paleoclimate reconstructions



Gabriel C. Rau^{a, b, *}, Mark O. Cuthbert^{b, c}, Martin S. Andersen^{a, b}, Andy Baker^b, Helen Rutledge^{b, d}, Monika Markowska^{b, e}, Hamid Roshan^{a, b}, Christopher E. Marjo^d, Peter W. Graham^{b, f}, R. Ian Acworth^{a, b}

^a Connected Waters Initiative Research Centre, UNSW Australia, 110 King Street, Manly Vale 2093, Australia

^b Connected Waters Initiative Research Centre, UNSW Australia, Sydney, NSW 2052, Australia

^c School of Geography, Earth and Environmental Sciences, University of Birmingham, Edgbaston, Birmingham B15 2TT, UK

^d Mark Wainwright Analytical Centre, UNSW Australia, Sydney, NSW 2052, Australia

^e Australian Nuclear Science and Technology Organisation, Lucas Heights, NSW 2234, Australia

^f SGA Environmental, Suite 8, 599 Pacific Highway, St Leonards, NSW 2065, Australia

ARTICLE INFO

Article history:

Received 22 December 2014

Received in revised form

23 March 2015

Accepted 28 March 2015

Available online 15 May 2015

Keywords:

Drip water temperature
Speleology heat transport
Paleoclimate archive
Speleometeorology

ABSTRACT

While several studies explore cave climate and thermal regimes, little is known about the controls on cave drip water temperature. Yet water temperature significantly influences biogeochemical processes associated with cave drips. To identify the processes that control the cave drip water temperature, we measured the temperatures at multiple locations along a speleothem flow path and drip sources (stalactites) concurrently with the drip rates in Cathedral Cave, Wellington, Australia. We monitored long-term drip water temperature, drip rates, surface and cave climate and in-cave evaporation rates and conducted 3 infiltration experiments with different flow, temperature and isotopic conditions. Our results show that the drip water temperature is controlled by multiple superimposed heat transport mechanisms that act upon the infiltrating water in the epikarst, the water film after it enters the cave and before it becomes a drip. The two main heat sources/sinks for drip water are the cave air and the surrounding rock. The subsurface temperature is coupled to the surface temperature by conduction through the soil and rock mass, but the cave climate is also coupled to the surface climate by venting. On a regional scale, drip temperatures are mainly driven by the annual ground surface temperature signal but damped with depth and shifted in time compared to the surface. On a local scale, the drip water temperature can differ significantly from cave air and speleothem temperature due to the latent heat exchange of evaporation and localised water film convection. The main controls are ground surface temperature, subsurface depth, air density induced ventilation, distance from entry and drip rate. We present a conceptual model that explains drip water temperature signals and provide signal driven guidance on best type and location for speleothem sampling. We anticipate that our results will significantly improve the understanding of temperature-dependent paleoclimate signals from speleothem archives.

© 2015 Elsevier Ltd. All rights reserved.

1. Introduction

1.1. Context and aims

Surprisingly little work has been done on what controls the temperature of cave drip water and yet this is of fundamental importance as it controls biogeochemical processes in caves. For example, drip water temperature influences the growth rate of speleothems (Dreybrodt, 1981; Baker et al., 1998), fractionation of

* Corresponding author. UNSW Australia, 110 King Street, Manly Vale, NSW 2093, Australia. Tel.: +61 2 8071 9850; fax: +61 2 9949 4188.

E-mail address: gabriel.rau@unsw.edu.au (G.C. Rau).

isotopes (Epstein et al., 1953), and deposition of biomarkers (Schouten et al., 2007). In speleometeorology, latent heat exchange processes such as condensation or evaporation alter the thermal energy content of drip water (De Freitas and Schmekal, 2003) and can lead to cooling of speleothems (Cuthbert et al., 2014a). Finally, in geomicrobiology, the habitat of cave microorganisms is strongly influenced by temperature (Northup and Lavoie, 2001).

Cave drip water originates from precipitation or surface flow, which infiltrates the soil surface. It is well recognised that the dynamic temperatures at the Earth's surface propagate into the subsurface (Stallman, 1965; Baker and Ruschy, 1993). Near-surface temperature measurements can be used to quantify water flow (Rau et al., 2014), for example by exploiting temperature–time variations (Taniguchi and Sharma, 1993; Bendjoudi et al., 2005) or temperature–depth profiles (Tabbagh et al., 1999; Cheviron et al., 2005). Fluctuating ground surface temperatures are damped with depth until a stable temperature is reached (Taniguchi, 1993; Smerdon et al., 2003). The dominant mechanism of subsurface heat transfer beyond the soil zone is by conduction (Smerdon et al., 2003). However, the influence of rock, as opposed to air, temperature profiles on cave drip water temperature has not been investigated.

Water commonly flows over speleothem surfaces such as flowstones, stalactites and draperies inside caves before arriving at the drip source (falling films) (i.e., Camporeale and Ridolfi, 2012). During film flow a number of different heat and mass transfer mechanisms act simultaneously. While the engineering literature reports on simultaneous heat and mass transfer during film flow (i.e., Yan and Soong, 1995), cave related sciences have not investigated the effects of film flow heat transport on the cave drip water temperature. Yet it is well accepted that water films will exchange moisture and heat with the cave air (Atkinson et al., 1983; Faimon et al., 2012).

Cave water is generally in contact with cave air for some time before forming drips. Cave climate must therefore be considered when investigating what controls cave drip water temperatures for caves that are open to the atmosphere. It has been shown that surface air temperature anomalies can affect cave air temperature (Dominguez-Villar et al., 2013, 2014). A change in cave climate is associated with advective air flow by venting (De Freitas et al., 1982; De Freitas and Littlejohn, 1987). Cave venting is caused by barometric pressure changes, density differences between cave and surface air (chimney effect) (Conn, 1966; Wigley, 1967; Oh and Kim, 2011) or through winds across the entrances (Venturi effect) (Kowalczyk and Froelich, 2010). Cave-atmosphere air exchange results in spatiotemporal variability of otherwise stable cave air temperature (Smithson, 1991; Perrier et al., 2010). In a comprehensive investigation of cave air venting Faimon et al. (2012) determined the key drivers of the microclimatic variability.

The cave climate also responds rapidly but predictably to changing atmospheric climate conditions (Atkinson et al., 1983; De Freitas and Littlejohn, 1987). Air flow can cause significant loss of water due to evaporation from caves (McLean, 1971) with increasing moisture loss for only small decreases in cave relative humidity below the saturation point (Buecher, 1999). Cuthbert et al. (2014a) reported significant cooling of speleothems, and drip water, through in-cave evaporation.

Conversely, cave condensation and its change to the overall thermal energy balance were also found to relate to cave air temperatures (De Freitas and Schmekal, 2003). Condensation can increase the temperature of cave walls (Dreybrodt et al., 2005). Further, considerable speleothem dissolution can be caused by condensation through the formation of calcite undersaturated drips (Tarhule-Lips and Ford, 1998). Importantly, cave climate exerts significant control on speleothem deposition through the

temperature dependence of both kinetic and equilibrium drip water geochemical processes (Spötl et al., 2005; Baldini et al., 2008). However, the in-cave climatic controls on cave drip water temperature have also yet to be explored systematically.

When considering temperature as a control for water related cave processes and the interpretation of temperature-dependent speleothem paleoclimate proxies, the cave air temperature is generally used, since it is easily measured. Here, we illustrate that the true cave drip water temperature can differ significantly from cave air temperature and we identify the processes exerting control. Hence the aim of this paper is to identify and describe the controls on cave drip water temperature. We systematically investigate the dominant influences on cave thermal regimes and drip water temperature by analysing subsurface heat (and mass) transport through the karst and the atmospheric connection. Examples for the different controls are presented using measurements of drip rate, speleothem and drip water temperature as well as climate data monitored inside the cave and on the land surface. Using this data we demonstrate how a surface air temperature climate signal will be propagated to a cave, and how the resulting drip water temperatures may deviate from the mean annual air temperature.

1.2. Description of the field site and prior work

Data presented in this paper was acquired at Cathedral Cave in the Wellington Caves Reserve (Latitude -32.622° , Longitude 148.940°) in New South Wales, Australia. Fig. 1 shows the location and horizontal dimensions of Cathedral Cave. Cathedral Cave is located in a temperate semi-arid zone. The Caves Reserve is exposed to a significant seasonal variation in the surface air temperature between approx. 0 to 45 °C, with a mean annual maximum temperature of 24.3 °C. Rainfall in the area is episodic, with a long-term annual value of 617 mm/year, and the relative humidity varies between 6 and 98% with a mean annual value of 68% (BOM, 2014).

The cave system is located in the Molong Anticlinorial Zone and intersects a massive and thinly bedded Devonian limestone (Osborne, 2007). Cathedral Cave is one of the larger caves featuring two nearby entrances and has a vertical depth of approx. 25 m. As a show cave it is well-developed with infrastructure suitable for tourist groups. The cave is easily accessible and offers an ideal opportunity to investigate subsurface karst processes, such as karst hydrology, geochemistry and paleoclimate signals in speleothems. The cave has been subject to long-term drip rate and drip water monitoring starting in 2009 and ongoing. Jex et al. (2012) correlated spatially distributed drip records and found that they group into distinct categories of differently behaving clusters indicative of the flow path features. Mariethoz et al. (2012) identified chaos in drip rates and concluded that this contains information about flow routing in fractured media. Rutledge et al. (2014) found clear soil and limestone signatures in the drip water through trace elements and organic matter analysis. Cuthbert et al. (2014b) reported that cave drip water is only activated after long duration and high volume rainfall, and that evaporation from the epikarst is an important control on drip water isotopic composition.

2. Materials and methods

2.1. Surface irrigation

Owing to the temperate semi-arid climate at the Wellington Caves Reserve, rainfall events sufficient to overcome the soil moisture deficit and trigger cave dripping are erratic (Jex et al., 2012; Mariethoz et al., 2012). To induce dripping in the shallow

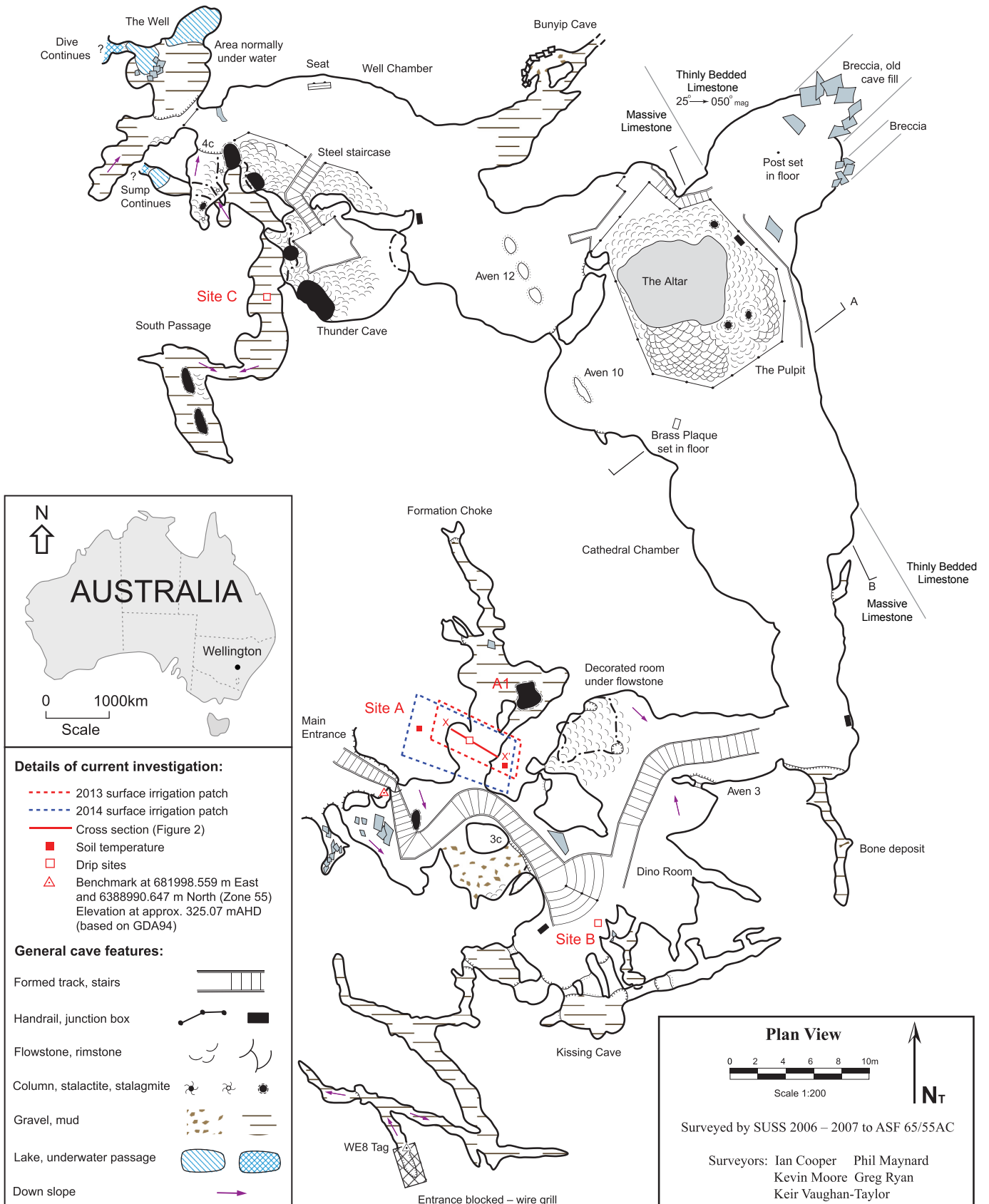


Fig. 1. Survey map of Cathedral Cave located in the Wellington Caves Reserve in NSW, Australia. Instrumented sites are marked with red on the map.

cave so that controls on cave drip water temperature could be investigated a total of 3 controlled surface irrigation experiments were conducted over a two year period (2013–2014). Geochemical results of the first irrigation experiment were previously published in Rutledge et al. (2014) and drip water temperature data from the second irrigation experiment has been reported in Cuthbert et al. (2014a).

During the surface irrigations a patch size of ~24 m² (2013) and ~50 m² (2014) above the near-surface chamber of Cathedral Cave (see Fig. 1) was hand hosed with town water from a storage tank. Two summer and one winter irrigation campaigns were conducted. The dates and specifics of each of the three surface irrigation experiments are summarised in Table 1. Importantly, during the first irrigation experiment, the temperature of first and third continuous surface application was set to approx. 0.3 °C using ice bags. Further, deuterium was added as a conservative tracer to the batch of water first applied (enrichment of ~6100‰ VSMOW) during surface irrigation in 2013. Markowska et al. (submitted for publication) provide a detailed analysis of the deuterium tracer measured during the same experiments as well as long-term monitoring of natural isotopic composition.

2.2. Cave and surface monitoring

Different sites were selected for monitoring at increasing cave depths and distance from cave entrance (Fig. 1). To measure the drip water temperature we affixed automated miniature temperature loggers (DST micro T, StarOddi, Iceland) along known flow paths of water on top of the speleothem (flowstone), with a logger mounted to the tip of the drip source (stalactite, Fig. 2B). The loggers were selected based on their small size, rapid temperature response time (~20 s), resolution (0.01 °C) and accuracy (±0.2 °C). These features make the loggers an ideal choice for monitoring drip water temperature. The cave air temperature was also measured in close proximity to the drip source (Fig. 2A). During the irrigation experiment in January 2013 (southern hemisphere summer) the shallow soil temperature of the irrigation patch was monitored at 2 locations with DST micro T loggers (Fig. 1).

In the January 2014 irrigations, in addition to the StarOddi loggers, detailed temperature measurements were acquired with high accuracy (±0.002 °C) and resolution (0.0006 °C) custom-built instrumentation. The sensors consisted of Platinum resistors (Pt1000, 1 kΩ at 0 °C) embedded in flat aluminium housing (25 × 6 × 1 mm – see Fig. 2C) designed for fast thermal response. Fig. 2 shows sensors deployed along a flow stone and stalactite near the entry (site A, location in Fig. 1). More details about method and results from this deployment are reported in Cuthbert et al. (2014a). Here, we use a subset of this data for a more detailed and comprehensive description of the heat transport processes that exert control on cave drip water temperatures.

The drip locations were also monitored continuously with automated drip counters (Stalagmate, Driptych, UK). Further,

climate monitoring stations consisting of relative humidity and temperature sensors (HMP155A, Campbell Scientific, USA) were deployed at 2 different locations to record the cave air. Cave barometric pressure was also measured using a pressure transducer (Levellogger, Solinst Inc., Canada). Water samples were regularly collected from drip sources at site A with 20 ml glass McCartney bottles. The samples were analysed using a Los Gatos[®] cavity ring down laser spectrometer with overall precision of ±2.0‰ δ²H. Evaporation pans (9.5 cm inner diameter) were deployed at site A and C (Fig. 1) for extended periods of time. Volumetric water loss was measured using a digital pipette, precision scale and the pan size, and the evaporation rate was calculated from the time of pan deployment.

Surface climate variables, i.e. air temperature, shallow soil temperature and moisture, relative humidity and barometric pressure, were monitored by a climate station (Hill Climate Station, Wellington, data download available: <http://groundwater.anu.edu.au/>) located in close proximity south-east of Cathedral Cave. Precipitation data was recorded by a rain gauge in Wellington ~6.5 km away (Agrowplow, station 065034) (BOM, 2014). The thickness of the soil zone was found to vary from 0 to 0.5 m estimated by inserting a thin metal rod into the soil across the irrigation patch. During the 2014 experiment volumetric soil moisture integrated across the upper 10 cm was measured frequently at random spots across the irrigation patch with a handheld meter (MPM160, ICT International, Australia).

2.3. Data processing

2.3.1. Surface to subsurface heat conduction

The Earth's surface is exposed to time variable heat influx from solar radiation, which forms a significant energy source for subsurface propagation. The periodicity of insolation is controlled through the Earth and solar cycles. Hence, surface air temperature contains distinct frequencies, i.e. daily, annual, decadal, centennial, millennial, as well as aperiodic environmental influences related to local weather and climate, i.e. high and low pressure systems, and oscillation indices. Cave temperatures have been related to ground surface and surface air temperatures by analysing heat propagation with depth through conduction assuming that thermal properties can be depth averaged (Smerdon et al., 2003, 2004).

Carlsaw and Jaeger (1959) formulated a 1D differential heat conduction equation. The equation was solved with a harmonic temperature boundary at the top and a constant temperature boundary at infinite depth. This resembles the subsurface environment between surface and cave. Since the heat transport equation is of linear nature, the analytical solution is valid for any harmonic component of temperature variation with an individual frequency (e.g. daily or annual) that is part of the total temperature signal (Goto et al., 2005).

Here, we consider that thermal diffusivity for soil can vary due to differences in saturation (Ochsner et al., 2001), compared to low

Table 1
Detailed summary of the individual surface irrigations conducted at 3 different times over a two year period between 2013 and 2014.

Date	Experiment/application	Water volume [litres]	Equiv. rain [mm]	Duration of irrigation [hours]	Equiv. rainfall intensity [mm/h]	Irrigation water temperature [°C]
8/01/2013	1/1	840	~35	1.75	~20	0.3
9/01/2013	1/2	1500	~63	1.75	~35	10.6
10/01/2013	1/3	840	~35	1.75	~20	0.3
11/01/2013	1/4	1500	~63	1.75	~35	24.2
14/01/2014	2/1	3400	~68	2.85	~24	~25
15/01/2014	2/2	2400	~48	3.00	~16	~25
22/07/2014	3/1	1460	~29	1.00	~29	~12
23/07/2014	3/2	745	~15	0.50	~30	~12
24/07/2014	3/3	1460	~29	1.00	~29	~12

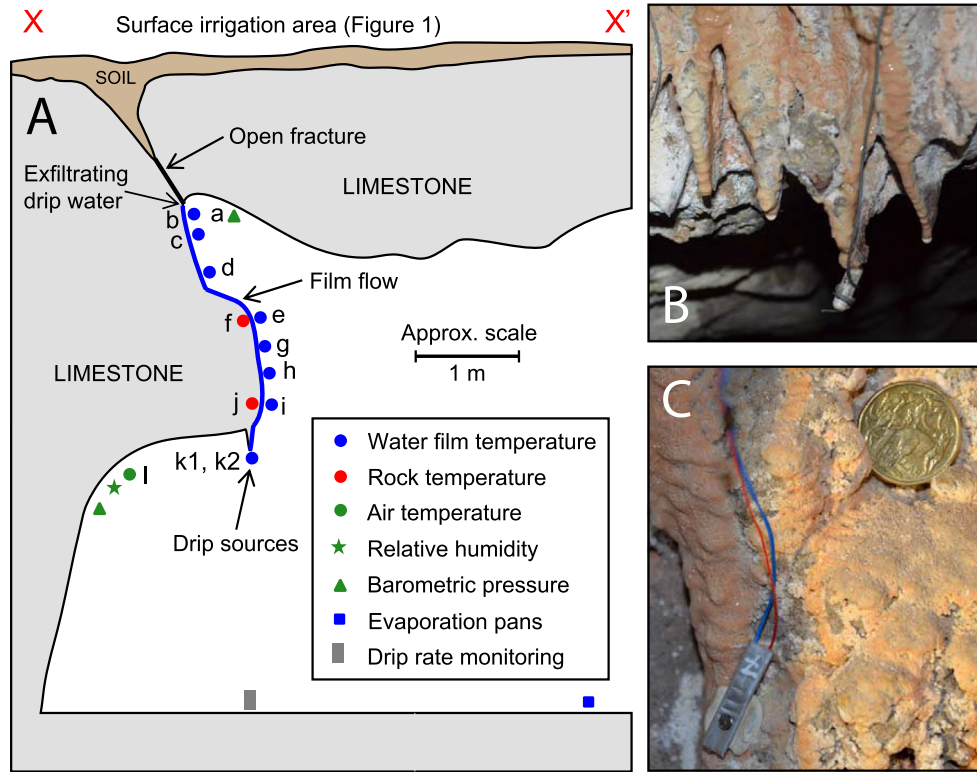


Fig. 2. A) Schematic subsurface cross-section of Site A (Fig. 1) showing the drip water flow path along a flow stone to the stalactite (drip site) and the sensors deployed to measure water film and drip temperature and cave air temperature as well as climate parameters (relative humidity and pressure). B) A StarOddi micro T temperature sensor measuring at the drip source. C) Example of high-precision aluminium temperature sensor mounted on flow stone along the flow path (Australian 1-dollar coin with 25 mm diameter for scale).

porosity bedrock which can be assumed to be constant over time. Consequently, it is useful to separate the subsurface into two layers: soil zone and epikarst zone. While several studies have used shallow multi-level soil temperature measurements to calculate near-surface infiltration (Smerdon et al., 2004; Bendjoudi et al., 2005; Cheviron et al., 2005) the propagation of thermal waves into rock above the groundwater table is predominantly controlled by thermal diffusion (Smerdon et al., 2003).

To calculate the dynamic subsurface rock temperature through two layers, an analytical solution (Carslaw and Jaeger, 1959; Goto et al., 2005) is modified as

$$T_i(z, t) = T_0 + A_i \cdot \exp\left(-\sqrt{\frac{\pi}{P_i}} \left(\frac{d_s}{\sqrt{D_s}} + \frac{z - d_s}{\sqrt{D_r}}\right)\right) \times \cos\left(2\pi \frac{t}{P_i} - \sqrt{\frac{\pi}{P_i}} \left(\frac{d_s}{\sqrt{D_s}} + \frac{z - d_s}{\sqrt{D_r}}\right) - \theta_i\right) \quad (1)$$

for $z \geq d_s$. Here, i is a distinct harmonic temperature component with period P_i [d]. T_i is the temperature [°C] due to harmonic temperature component i as a function of depth z below subsurface [m] and t is time [d]; T_0 is the mean surface temperature [°C]; A_i is the amplitude [°C] of the harmonic signal i ; θ_i is a phase offset [rad]; d_s is the thickness of the soil layer [m].

In Equation (1), D is the effective thermal diffusivity for the soil layer (subscript s) and the epikarst (subscript r). In general, the thermal diffusivity [m²/d] is defined as (Carslaw and Jaeger, 1959)

$$D = \frac{\kappa}{\rho c} \quad (2)$$

where κ is the bulk thermal conductivity [W/m/K] for variably saturated soil or solid rock (De Vries, 1963; Horai, 1971; Clauser and

Huenges, 1995; Tarnawski et al., 2011). Analogously, the bulk volumetric heat capacity ρc [MJ/m³/K] is reported for sediments and rock (Schön, 1996; Schärli and Rybach, 2001).

Equation (1) can be used to predict the subsurface temperature response to a particular frequency component of interest extracted from the ground surface temperature data. For example the i -th component could be daily, annual, centennial, millennial, or any other significant component determined using a Fourier transform analysis of dominant frequencies. In Equation (1) the exponential part accounts for temperature amplitude damping and the cosine part for the shift in phase over depth. The phase offset θ is the time relative to the maximum insolation (summer solstice on 21 December in the southern hemisphere) and accounts for any difference between the conduction theory and realistic conditions.

In this paper we use 2 different layers, one representing the soil and one the limestone. We measured the thermal conductivity and heat capacity of soil and limestone samples collected at the Cathedral Cave field site (Fig. 1) using a KD2 Pro thermal analyser (Decagon Devices, US). To account for the variable water saturation of the soil (i.e. dry and saturated end members), the soil parameters were measured after oven drying (105 °C, 6 h) and after saturating the soil sample with water. Further, a piece of limestone bedrock had holes drilled for inserting the instrument needles, and a highly conductive paste was used to ensure optimal thermal bridging between needle and limestone sample. The measured thermal parameters are listed in Table 2.

Equations (1) and (2) were used to simulate the annual temperature variations (with $P = 365.25$ d) at various depths of interest. Models were fitted to temperature observations by varying parameters as outlined in Table 4 and minimising the normalised root mean square error (NRMSE). For the surface air temperature the parameters of interest were mean annual temperature (T_0),

amplitude (A) and phase offset from solstice (θ) while the depth was set to zero ($z = 0$). For the cave air and flowstone temperatures the parameters of interest were mean annual temperature (T_0), depth of limestone (z) and phase offset (θ). Here, the remaining parameters were set as follows: Amplitude A as determined from the surface air temperature fit, soil zone thickness $d = 0.1$ m, thermal diffusivities as measured on soil and a limestone sample (Table 2).

2.3.2. Air density calculation

A well-known process of cave atmosphere air and moisture exchange is venting stimulated by the difference in density between atmospheric and cave air (the chimney effect) (Conn, 1966; Wigley, 1967; Oh and Kim, 2011). The density of air can be calculated taking into account thermodynamic properties of dry air as well as water vapour (Giacomo, 1982). It is expressed as

$$\rho_a = \frac{pM_a}{ZRT} \left[1 - x_v \left(1 - \frac{M_v}{M_a} \right) \right] \quad (3)$$

where p is the barometric pressure [Pa]; Z is the compressibility coefficient, under the conditions reported here of value 0.999611566 [–]; R is the universal gas constant, 8.31441 [J/K/mol] and T is the temperature [K]; M_a and M_v are the molar mass of dry air 0.0289635 [kg/mol] and water vapour 0.018015 [kg/mol]. The mole fraction of water vapour in moist air x_v is defined as

$$x_v = \frac{h}{p} \exp(AT^2 + BT + C + DT^{-1})f \quad (4)$$

where h is the relative humidity ($0 < h < 1$); f is an enhancement factor, under the conditions reported here of value 1.0038 [–]; the saturation vapour pressure coefficients are published as $A = 1.2811805 \cdot 10^{-5}$ [K⁻²], $B = -1.9509874 \cdot 10^{-2}$ [K⁻¹], $C = 34.04926034$, $D = -6.3536311 \cdot 10^3$ [K]. For above parameter values please refer to Giacomo (1982).

Equations (3) and (4) require measurement of the common variables that define the thermodynamic state of moist air: barometric pressure, air temperature and relative humidity (RH). To investigate cave venting, air densities were calculated from the surface and cave climate records for a 2-week period during both summer and winter in 2014.

3. Results

3.1. Surface and cave climate

Fig. 3 shows surface air temperature and rainfall recorded at the surface above Cathedral Cave over a 2-year period between 2012 and 2014. Cave air temperature measured near site A is also shown.

Table 2
Summary of thermal parameters of water, air, soil and limestone.

Material	Thermal conductivity [W/m/K]	Specific heat capacity [MJ/m ³ /K]	Thermal diffusivity [m ² /d]	Min. thermal diffusivity [m ² /d]	Max. thermal diffusivity [m ² /d]
Water @ 18 °C	0.595 ^a	4.180 ^a	0.0123 ^a	–	–
Air @ 18 °C	0.025 ^a	0.001 ^a	1.8014 ^a	–	–
Soil (dry)	0.545 ^b	1.188 ^b	0.0396 ^b	–	–
Soil (saturated)	0.835 ^b	2.939 ^b	0.0245 ^b	–	–
Soil	–	–	0.03 ^c	0.01 ^c	0.06 ^c
Limestone	2.356 ^b	2.518 ^b	0.0808 ^b	0.06 ^c	0.14 ^c

^a Water and air properties can be found in NIST (2014).

^b Soil and limestone properties were measured in the laboratory using samples collected in the field.

^c Ranges for soil thermal parameters and limestone bedrock are from Ochsner et al. (2001) and Vosteen and Schellschmidt (2003).

Table 3
Cave evaporation rates measured at different locations and opposing seasons.

Location	Evaporation rate [mm/year]	
	Summer (January 2014)	Winter (July 2014)
Near entrance	440	
Site A	50	>56
Site B	40	
Site C	13	4.8

A climatic summary for the period between Jan 2013 and Dec 2014 is as follows: The minimum and maximum surface air temperatures were -2.9 °C and 43.5 °C. Typical for a temperate semi-arid climate, relative humidity varied between 5 and 98%, with a median of ~63%. For more than half of the year (233 d) the volumetric soil moisture content was below the median annual value of 21% because evapotranspiration generally exceeds precipitation.

While ~312 days/year were without significant rain (<1 mm/day), a below average yearly total of 550 mm was recorded from episodic rainfall events occurring on 86 days/year. On 1 March 2013 a maximum daily rainfall of 74 mm was recorded. The amount of rain from this natural event was comparable to the manual application of water on the irrigation patch during the surface irrigation experiments (Table 1 and Fig. 1).

At Site C, the air and speleothem temperature was very stable at 17.8 °C with only minor fluctuations of ~0.1 °C between January–December 2014. Cave relative humidity (RH) was measured at 10 min intervals during parts of the year between January and November 2014. The RH, recorded at site A, fluctuated significantly with minimum, maximum and median values of 59.3%, 97.9% and 88.6%, respectively. At site C the RH showed very minimal fluctuations around a median value of 97.1%, with minimum and maximum RH of 96.5% and 97.8%, respectively. Evaporation rates as measured at the different locations (Fig. 1) during summer and winter 2014 are shown in Table 3. There is a clearly decreasing trend in evaporation rate with increasing distance from entrance in summer, with RH values increasing as expected. Noteworthy, however, is the stable but below saturation RH level at site C leading to some potential for evaporation from the deepest part of the cave throughout the year.

3.2. Drip water temperatures during irrigation experiments

Fig. 4 presents high resolution temperature measurements, drip counts and relative humidity measured during irrigation experiment 2 conducted in January 2014 (summer). While the majority of the measurements in Fig. 4 were previously published by Cuthbert et al. (2014a), we use this dataset as a starting point and present new results that reveal a detailed analysis of the different controls on cave drip water temperature.

Table 4

Summary of results obtained by analysing temperature data from different locations with Equation (1) using an annual signal period ($P = 365.25$ days), soil zone thickness $d = 0.1$ m (except for surface air temperature), soil and limestone thermal diffusivity listed in Table 2. Phase offset is relative to summer solstice. The fitting algorithm minimised the NRMSE by varying the bold parameters.

Temperature measurement location	Mean	Amplitude	Phase	Phase offset	Total depth	NRMSE	Number of data points
Parameter [unit]	T_0 [°C]	A [°C]	[d]	θ [d]	z [m]	[–]	[–]
Surface air	16.90	8.51	0	20.0	0	0.1827	52,376
Flowstone (b, Site A)	17.18	5.03	30.7	31.9	1.55	0.2579	30,810
Flowstone (c, Site A)	16.62	4.11	42.4	31.8	2.16	0.2341	30,811
Stalactite (j, Site A)	16.11	2.61	68.8	31.2	3.55	0.1653	30,814
Cave air (Site A)	16.32	2.38	74.1	31.4	3.83	0.3609	23,750
Cave air (Site A1)	15.70	1.65	95.6	31.1	4.95	0.3400	29,338
Cave air (Site C)	18.10	–	–	–	~25	–	17,959

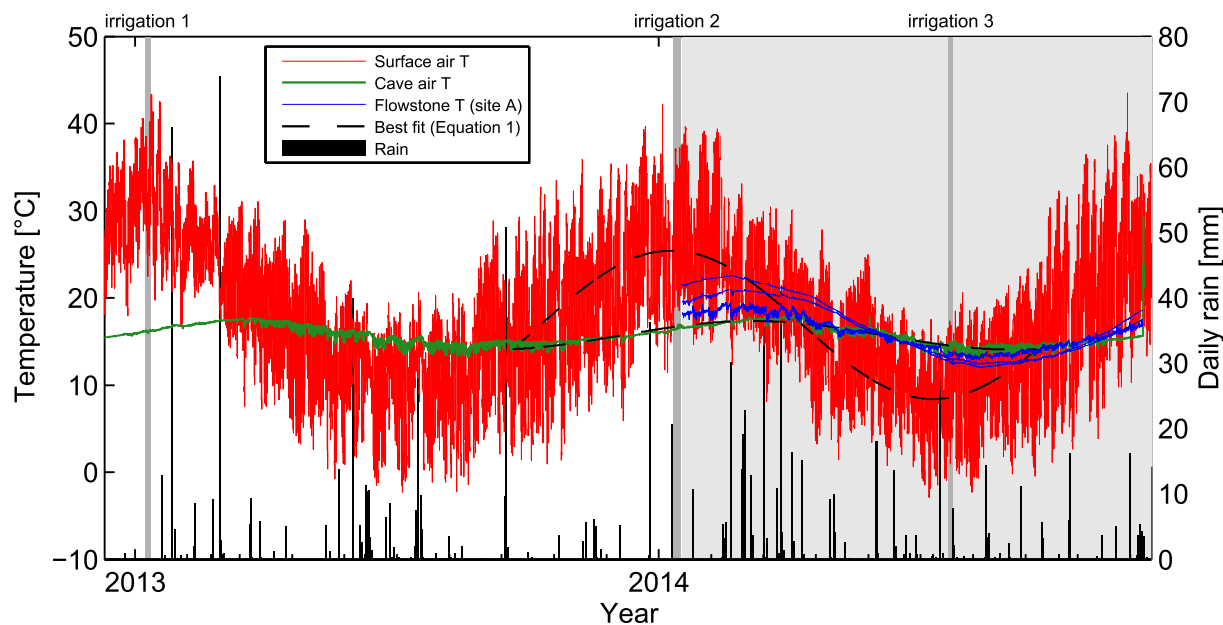


Fig. 3. Data from two years of monitoring at the Cathedral Cave: Surface air temperature, daily precipitation, and cave air temperature (measured at Site A1 Fig. 1). For air temperatures, best fit to Equation (1) is indicated by dashed black lines. Blue lines are the drip water temperatures measured at Site A. Vertical dark grey bars show the times at which surface irrigation experiments were conducted coinciding with intense data collection periods. The light grey background indicates the times at which longer-term cave flowstone and drip water temperature was measured. The blue lines are speleothem and drip water temperature measurements enlarged in Fig. 6 and explained later.

Before the first surface irrigation the soil moisture across the irrigation patch was between 4 and 24% indicating a high soil moisture deficit. Approx. 3 h after the start of the water application (~68 mm rainfall equivalent) the drip source responded with a rapid increase to approx. 140 drips/min (Fig. 4B). Before the second irrigation the soil moisture was much higher with measurements ranging between 20% and 37%. After applying less water in the second irrigation (equivalent of ~48 mm rain) the drip source responded much quicker (~1 h after start) and showed significantly faster drip frequency (~180 drips/min) and longer drip activity compared to the previous day (Fig. 4B).

Before the onset of dripping, temperature measurements taken on the dry speleothem surface along the expected drip water flow path (Fig. 2A) were relatively constant in time but with decreasing temperature from cave ceiling to drip source (stalactite) revealing a downward gradient approx. -0.8 °C/m (Fig. 4A). Measured air temperatures reflect a spatial gradient that was similar to the one measured on the rock surface. Relative humidity measurements (RH) varied between a minimum of 79% and a maximum of 91.5%. A spot measurement near the chamber ceiling revealed RH of up to 98% after the flowstone had been wet at the end of the irrigation experiment in Jan 2014.

Temperatures, measured after activation of cave dripping, exhibit a rapidly increasing temperature on all sensors, peaking at

approx. -0.3 – 0.8 °C above the original measurement coinciding with a peak at the maximum drip count (Fig. 4A). This is followed by a slow temperature decrease as the drip rate decreases. At ~20 drips/min, the drip water temperatures measured by the lower sensors returned to the level measured before the onset of flow.

After a period of relatively stable measurements, the drip water temperature started to decrease, with lower sensors showing a more rapid and pronounced cooling of up to 1.5 °C below the cave air temperature which was measured in close proximity. The onset of observable evaporative cooling was at a RH of 90%, and the increase in drip water cooling coincided with a rapid drop of RH to 79%.

After the second surface irrigation the same temperature increases were observed but with stronger magnitude and longer duration, despite the application of less water at the surface. However, evaporative cooling was less pronounced reflecting the higher levels of RH (85–90%) during this event compared to the first event.

Fig. 5 summarises temperature and deuterium data as well as drip counts measured during irrigation experiment 1 conducted in January 2013. Note that the experimental procedure and measurement setup differed compared to experiment 2 described in the last section. Here, drip water temperature was only measured at the drip source (same stalactite as above). However, in addition

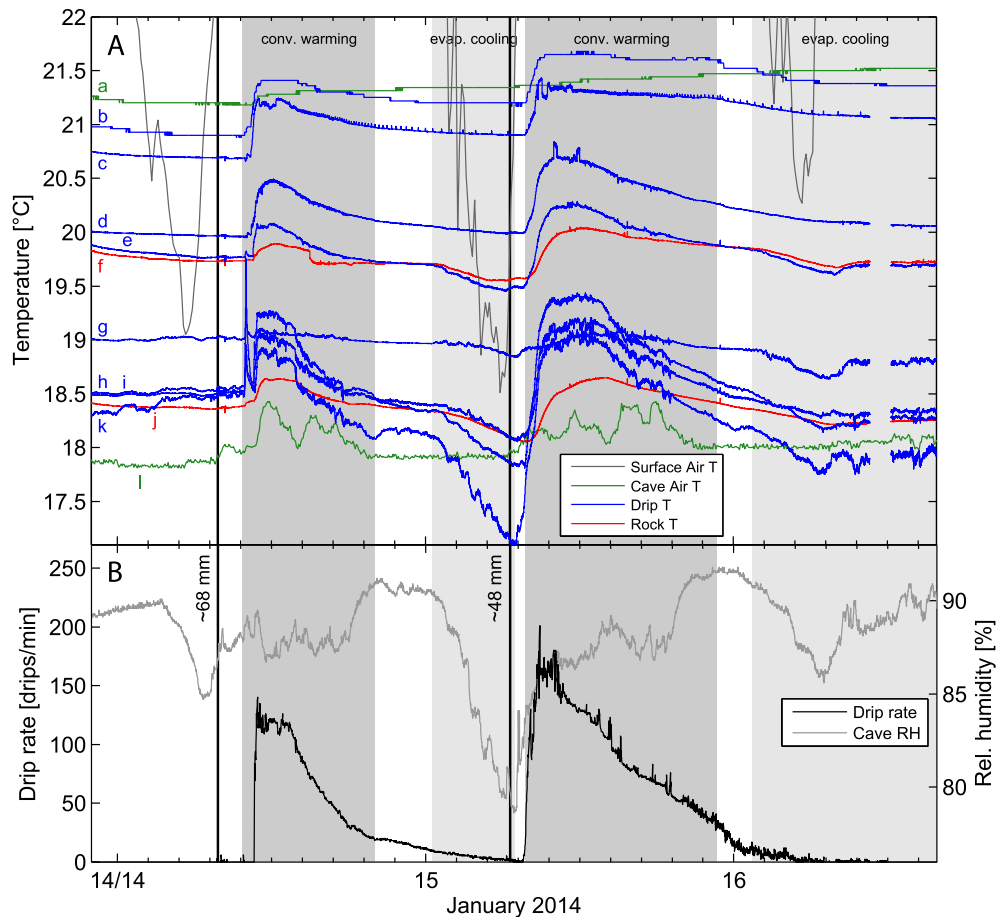


Fig. 4. Drip monitoring with high time-resolution at site A during summer 2014. A) Temperature measured along a drip water flow path (for locations see Fig. 2A) on top of the flowstone (blue), at ~40 mm depth into the flowstone (red) and in the air (green). Surface air temperature is also plotted (grey). B) Drip rate and relative humidity. A total of 2 irrigations were conducted (vertical black lines indicating equivalent rainfall) with 3400 L and 2400 L applied to the surface irrigation patch. Parts of this data were previously published in Cuthbert et al. (2014a) to demonstrate evaporative cooling of speleothems. Light grey shaded areas indicate periods dominated by evaporative cooling. Dark grey shaded areas depict periods dominated by film convection.

shallow soil temperatures (~5 cm and ~10 cm below the surface) were measured, but cave air RH was not. It is noteworthy that 4 individual irrigations were applied (35–63 mm rainfall equivalent) and with the water during the first 3 applications cooled to ~0 °C, ~10 °C and ~0 °C, respectively.

Cave air temperature was relatively stable at approx. 17.5 °C (Fig. 5A), while the daytime outside air temperature peaked at approx. 40 °C. During the time of experimentation the cave air temperature shows slight increases during the times at which the surface air temperature was at its lowest (night time). This excludes one occasion on 10 January 2013 where the cave air and drip water temperatures both decreased coincident with the surface air temperature falling below the average cave temperature (grey arrow in Fig. 5B). Also noteworthy here is the response of the soil temperatures to the cooled irrigation water, with both sensors showing measurements as low as 5 °C and 14 °C which are clearly below the minimum surface air temperature of 15 °C during that time (Fig. 5A).

Drip water temperatures responded similarly to the surface irrigation during the January 2013 experiment (Fig. 5D) compared to the experiment in 2014 (Fig. 4B). Interestingly, the drip water temperature at the first drip activation with an average drip response of 80 drips/min shows a cooling event during which there was a significant temperature difference of ~2.5 °C between drip water and air temperature (Fig. 5B). This was the response to an

irrigation application where the water was cooled to 10 °C, less than during the first irrigation (Fig. 5A). A similar sized evaporative cooling event can be seen again during the drip recession caused by the last surface irrigation where ~24 °C water was applied without the addition of ice. A clear deuterium enrichment (deuterium breakthrough) was measured in drip water samples after the third surface application originating from the deuterium that was added to the first irrigation batch (Fig. 5C).

Drip water temperature after the third surface irrigation during which water was cooled again to 0 °C showed a very small decrease before warming and tracking close to the cave air temperature (Fig. 5B). As soon as the drip rate fell below ~30 drips/min another evaporative cooling event was observed. This time, however, it was overwhelmed by the last surface application of water which carried warm water as film flow along the speleothem surface.

3.3. Long term air, speleothem and drip water temperature records

Fig. 6 shows the temperature data measured on the speleothem surface (dry or wet cave over speleothem surfaces) at three different locations along the drip water flow path at site A (see Fig. 2) including the drip source (stalactite), air temperature and drip rate over a time period of ~11 months. Fig. 6 includes the response to surface irrigation experiment 3 (also highlighted in Fig. 3). The trend in all temperature data complies with a distinct

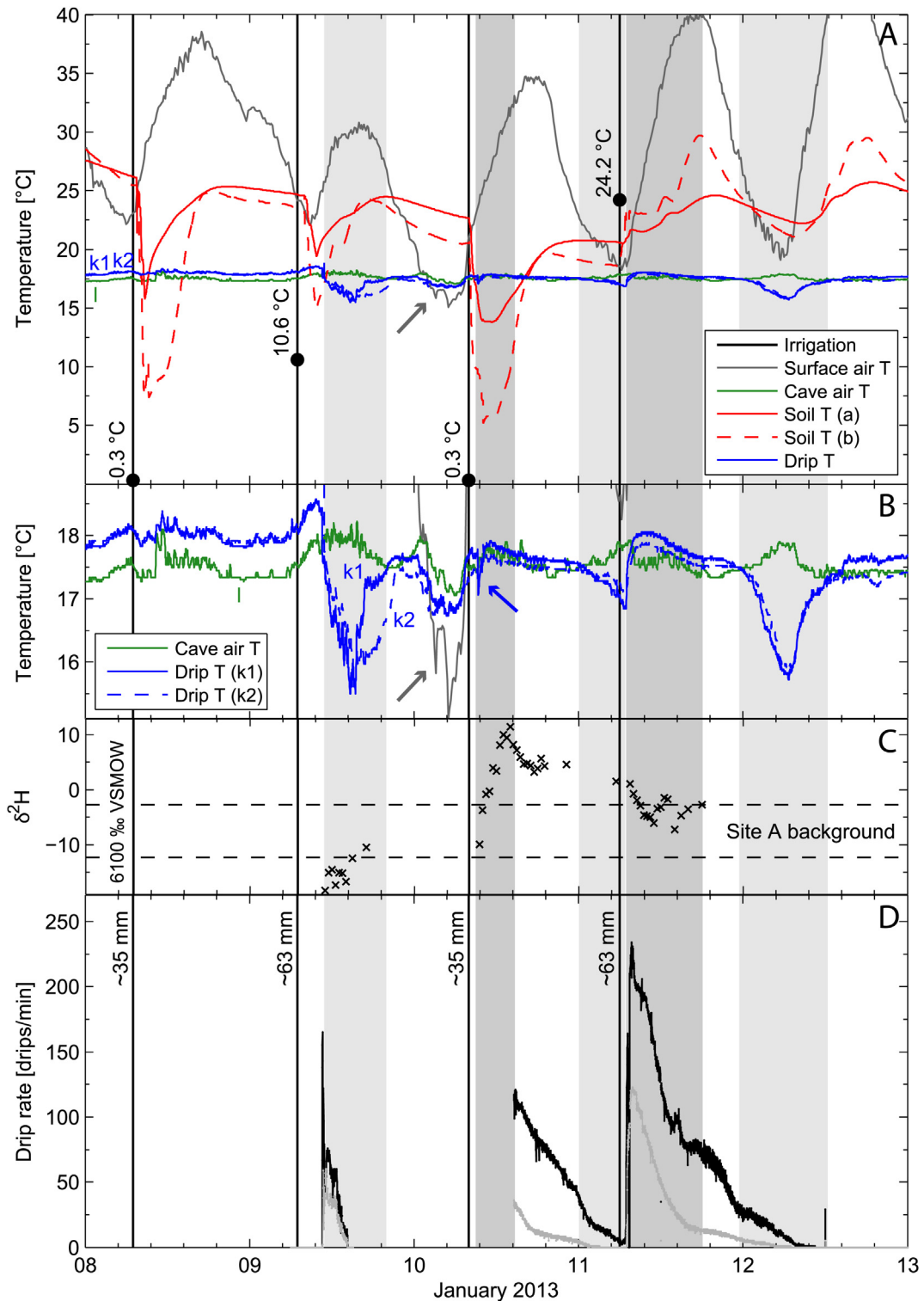


Fig. 5. Drip monitoring with high time-resolution at site A during summer 2013. A total of 4 irrigations were conducted with rainfall equivalents of 35 mm and 63 mm. A) Temperature measured at the tip of two neighbouring stalactites, and in the air (see Fig. 2 for locations). Irrigations 1, 2 and 3 were cooled using bags with ice (irrigation water temperature is indicated next to the vertical black lines in a). B) Vertically enlarged temperature data from A. C) Deuterium measured in drip water samples during the irrigation experiment. Deuterium was added to the first irrigation (-6100‰ VSMOW). Min/max of the 2-year average from various drip sources at site A (Markowska et al., submitted for publication). D) Drip rate of both stalactites. The grey arrow (A and B) depicts the time when the surface air temperature was lower than the cave air temperature indicating cave venting. The blue arrow (B) shows the time at which the cooled surface irrigation caused a drip water temperature anomaly. Light grey shaded areas indicate periods of evaporative cooling. Dark grey shaded areas depict periods of film convection.

annual harmonic but with different amplitude and phase compared to surface air temperature. This originates from subsurface conduction of the annual surface temperature wave, and we will refer to this as the “background temperature”.

Results from fitting surface air, cave air, speleothem and drip water temperature–time-series to Equation (1) with an annual periodicity are presented in Table 4 ordered by increasing total depth. The best fitting annual harmonics are also plotted in Figs. 3 and 6. Noteworthy here is the characteristic amplitude damping and phase shifting with increasing total depth. While the surface air temperature is offset from summer solstice by 20 days, there is a relatively constant phase offset of ~11–12 days (compared to the surface air temperature) once the annual temperature harmonic propagated through the subsurface. This indicates compliance with the subsurface heat conduction theory (Equation (1)). Further, total depths obtained from the fitting procedure are in good agreement with the vertical cave dimensions estimated from an in-cave survey (Fig. 2A).

The two upper measurement points show relatively stable temperature over time, when considering faster than annual frequencies, but with occasional upward and downward spikes indicating fast advective film flow in summer and winter, respectively. However, the temperature measured in air and the tip of the stalactite (Fig. 2) shows marked fluctuations with a daily frequency and varying amplitude of up to ~1 °C superimposed on irregular lower frequency variations and the background temperature. A number of drip events with varying magnitude and with a maximum of ~25 drips/min were recorded (Fig. 6). At this point a question arises: What causes the faster than annual temperature fluctuations?

3.4. Examples of venting induced drip temperature changes

Fig. 7 shows a detailed snapshot of cave flowstone, 2 stalactites, and cave air temperature (A, D) as well as cave RH (B, E), and surface and cave air density calculated using Equations (3) and (4) (C, F) during summer and winter in the year 2014.

In summer (Fig. 7A–C), a small drip event triggered an upwards temperature spike ~0.5 °C on the stalactite, followed by multiple

cooling fluctuations with magnitude ~1.5 °C coinciding with rapid decreases in cave air RH due to the venting events. A decrease in cave air temperature, with some delay, as a result of evaporative cooling, is also evident from the data. The cooling events are similar to those observable during the irrigation experiments (Figs. 4A and 5A) but seem to occur with a daily frequency over certain periods (Fig. 6). When comparing this with the surface and cave air densities it is clear that the regular RH decreases correlate well with periods where the surface air is denser than the cave air (note that dry air is denser than humid air of the same temperature) in the early mornings causing frequent cave venting events. Interestingly, evaporative cooling dips also occur higher up the profile where the drip water flows as a film along the speleothem surface (Fig. 6).

Fig. 7D–F contains the 2 weeks of winter monitoring that also coincide with the third surface irrigation experiment 3. In winter (Fig. 7D–F) the drip source shows regular daily temperature fluctuations of ~0.8 °C. Inspection of cave climate parameters reveals that the cave air temperature fluctuates more and the RH less compared to summer (Fig. 7E vs B). Further, the outside air is almost continuously denser than the air in the shallow entrance area (Fig. 7F). Interestingly, the drip water temperature mainly reflected the pattern of the cave air temperature while the drip rate (resulting from artificial surface irrigation during winter) did not exceed ~25 drips in a 15 min interval.

4. Discussion

Results presented in this paper allow, for the first time, a detailed identification of what controls the temperature of cave drip water. First we identify the controls and analyse how they affect drip water temperature, then we discuss their significance and implications in relation to interpreting speleothem records as paleoclimate archives.

4.1. What mechanisms control the cave drip water temperature?

Water movement to the drip source often occurs as film flow on cave deposits along variable distances (Dreybrodt et al., 2005; Camporeale and Ridolfi, 2012; Baker et al., 2014). The data

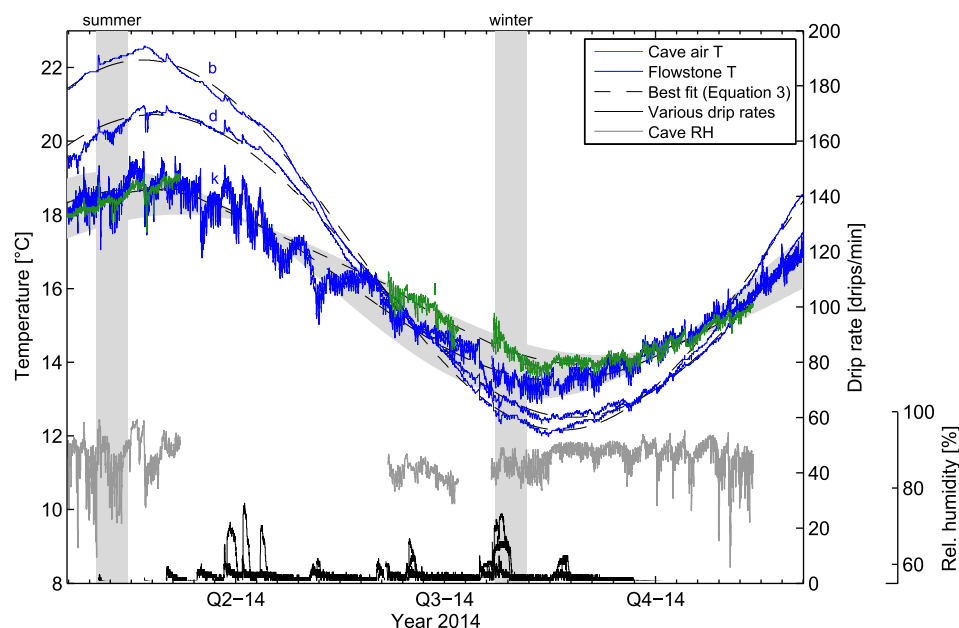


Fig. 6. Temperatures measured at Site A on the flowstone surface where film flow occurred during times at which the drip source is active. Locations of the records are marked according to Fig. 2. Data framed by grey vertical bars are highlighted in Fig. 7. The highlighted winter dataset coincides with the surface irrigation experiment 3 (see also Fig. 3).

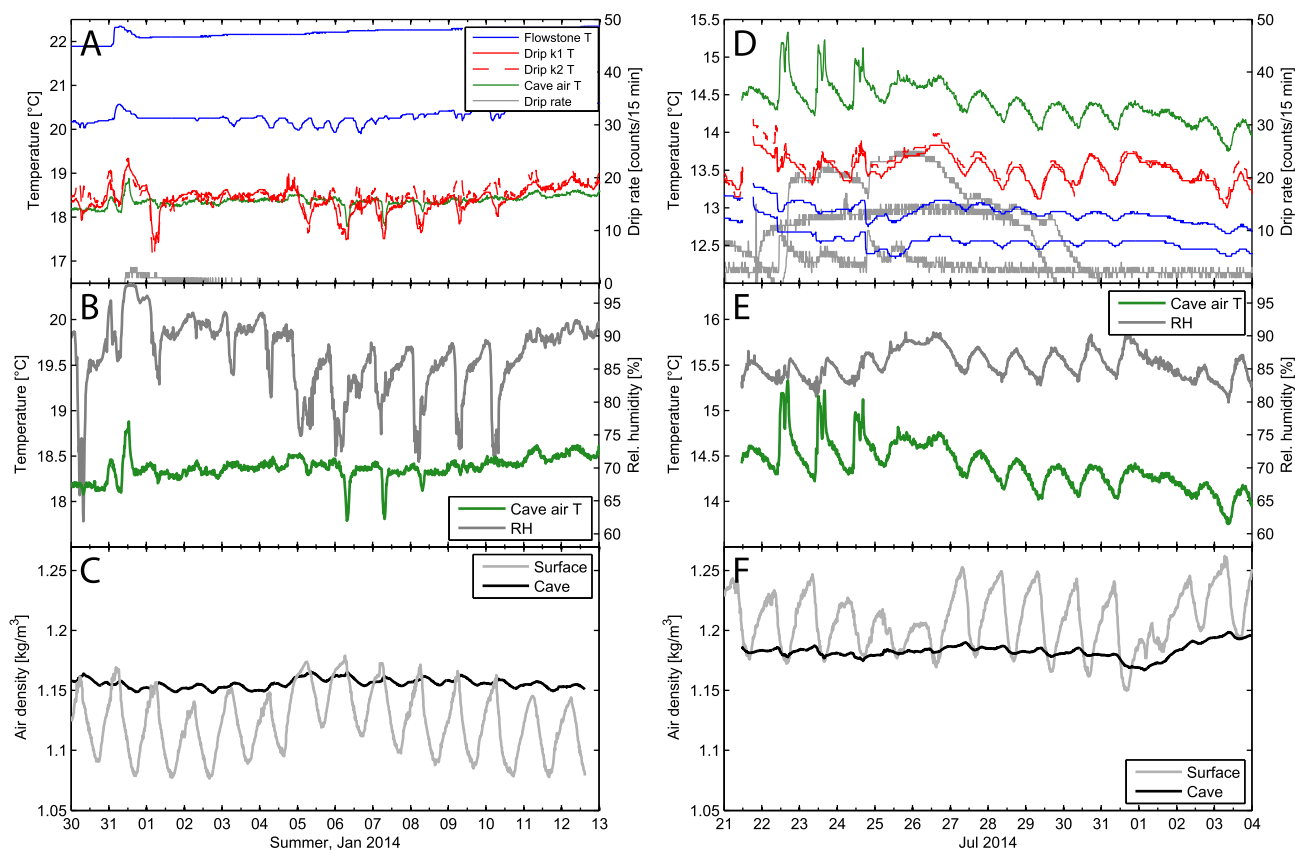


Fig. 7. Summer (A–C) and winter (D–F) snapshots of dry/wet speleothem and cave air temperature (A and D), cave climate (B and E), surface and cave air density (C and F). Note that the winter dataset (D–F) shows the response to surface irrigation experiment 3 (see Fig. 3). Note that y-axes of subplot B, C, E and F have the same range for better signal comparison.

presented here demonstrates that cave drip water temperature is controlled by a number of simultaneous heat transport mechanisms that act upon the water film. Heat transfer between rock and water in karst conduits was analysed in detail by Covington et al. (2011), Covington et al. (2012) and Luhmann et al. (2015). Dreybrodt et al. (2005) have theoretically analysed the heat and mass interactions involved in condensation corrosion involving water films. The engineering literature has recognised the complexity of film flow heat and mass exchange (i.e., Yan and Soong, 1995). In relation to speleology our results are first in reporting and analysing heat transport processes that control cave drip water temperature.

The variety of different mechanisms and associated variables complicates quantification of the individual processes. Here, we focus on a detailed description of temperature characteristics that can be measured after water enters the cave and flows along cave features before arriving at the drip source. Fig. 8 conceptualises the controls on drip water temperature. The individual heat transport mechanisms are discussed with reference to examples presented in the results.

4.1.1. Convective heat transport

4.1.1.1. Heat convection due to subsurface water percolation ($q_{f,surf}$)

During the first surface irrigation experiment the water was deliberately cooled (Table 1) to test whether its thermal signature, transported by heat convection through the soil zone and the epikarst stores, is detectable at the drip source. The pre-existing large soil moisture deficit prior to surface irrigations was responsible for the first irrigation not producing any flow in the cave

(Fig. 5A). Due to the hot weather and general heat conduction towards the irrigated patch the cooled soil recovered to near normal temperatures between each of the cooled irrigations. While the second application was cold enough ($\sim 10^\circ\text{C}$) for the thermal signature to be seen in the soil zone the cooling anomaly observed at the drip source (locations k1 and k2 in Fig. 5B) did not originate from the cooled surface irrigation. The main evidence for this conclusion is the lack of breakthrough of the deuterium enriched water ($\sim 6100\%$ VSMOW) from the first irrigation (Fig. 5C). The breakthrough of deuterium occurred after the third irrigation, indicating that the water travel time was significantly longer than the time between individual irrigations and the corresponding drip response in the cave. Markowska et al. (submitted for publication) concluded that the water activating the drip came from epikarst stores. This also means that convection of cold water from the surface to the cave will take longer than the individual drip response time.

While the soil zone clearly responded to the three applications of cooled water at 2 separate locations (Fig. 5A), the only signature attributable to the ice water detected at the drip source was a sharp short temperature fluctuation of only -0.8°C on 10 Jan 2012 at 09:18 while the air temperature remained constant (blue arrow in Fig. 5A). Importantly, this happened at a time during which fast film flow occurred over the flowstone, so this is not a temperature signal attributable to evaporative cooling (which only is dominant at slower flow). Interestingly, this short lasting cooling event was detected shortly after the start of the third surface irrigation (~ 35 mm rainfall equivalent) with ice-cooled water ($\sim 0^\circ\text{C}$) while the soil was still cooled from the previous event. We interpret this as *heat convection due to subsurface water percolation* caused by fast

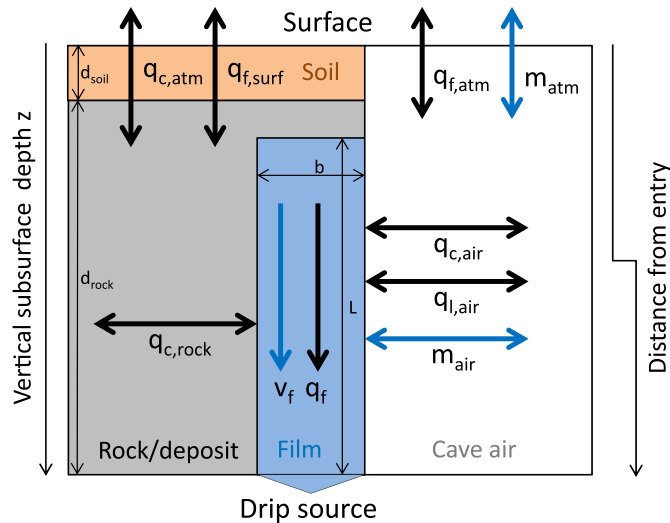


Fig. 8. Conceptual model of the different controls on cave drip water temperature between surface and drip source. Individual heat and mass transfer mechanisms are depicted by arrows and described as follows: $q_{c,atm}$ is conduction between surface and subsurface, $q_{f,surf}$ is convection between surface and subsurface, $q_{f,atm}$ is convection between surface and cave air, m_{atm} is moisture exchange between surface and cave air, $q_{c,rock}$ is conduction between speleothem and water film, $q_{c,air}$ is conduction between water film and air, $q_{l,air}$ is latent heat exchange between water film and air, m_{air} is moisture exchange between water film and air, q_f is convection of the water film, v_f is advection of the water film, L is the film flow distance between water entering the cave and drip source, b is the thickness of the water film.

preferential flow through the well wetted soil and fracture flow in the epikarst below. Note that first breakthrough of deuteriated water from the first surface irrigation was observed at the same time (Fig. 5C and Markowska et al., submitted for publication).

The above discussion illustrates that drip water temperature can be affected by thermal energy transported from the surface to the drip source through convection caused by *subsurface water percolation*. However, the prerequisites are that soil moisture is at field capacity, that preferential flow paths are still present and that the volume of water applied to the surface is much larger than the likely event based rainfall (105 mm was the maximum event based total between Oct 2011 and Dec 2014). In our case it took more than 133 mm rainfall equivalent (3 irrigations) of cooled water to produce a brief and small temperature anomaly. Furthermore, the experimental conditions were a worst case scenario in two other ways: 1) the temperature difference between the cooled irrigation water and the soil of 20–25 °C was unrealistically large for natural conditions, and 2) the section of the Cathedral Cave used in these experiments is very shallow with only about 1.7 m of soil and rock mass between the cave ceiling and the surface.

We expect that *heat convection from subsurface water percolation* caused by preferential flow through the soil and fracture flow through the epikarst can rarely cause drip water temperature anomalies that are significant for paleoclimate reconstructions from speleothems under realistic conditions. However, we acknowledge that this will depend on the thickness of the soil and epikarst as well as the fracture network above the cave. More research is needed to determine the conditions for which heat convection due to preferential or fracture flow from the surface can cause temperature anomalies that are of significance for speleothem-based paleoclimate reconstructions at drip sources.

4.1.1.2. Heat convection (q_f) due to film advection (v_f) along fractures and cave walls

The mechanism of convective heat transport *due to film advection* is clearly illustrated in the drip water temperature response

during surface irrigations 1 and 2 (see labelled areas in Figs. 4A and 5B). Since it is summer, warmer water flows in films along the speleothem surfaces (v_f) where the thermal signature from above is carried with the water film (q_f) (Figs. 4A and 5A). As a result of convective heat transport due to film advection the drip water temperature was raised by ~1 °C, but only at the start of the irrigation response (fastest drip rates on an event basis, here >50 drips/min) and when a negative temperature–depth gradient existed (i.e., summer).

Temperature sensors located in the upper part of the profile (location b and c in Fig. 2A) near the point at which water enters the cave detected a warmer water film compared to the surrounding air (Fig. 4A). This thermal disequilibrium indicates heat convection due to fast preferential or fracture flow triggered by the surface irrigation (Cuthbert et al., 2014a). However, it is important to note that the thermal energy causing the warming anomalies does not originate directly from the water applied to the surface. Instead, the anomalies originate from conduction between water film and rock higher up along the profile (explanation further below). Convective breakthrough between surface and cave only occurred under extreme circumstances, as pointed out in the previous subsection. The warming anomalies express a temporary downward shift of the localised conductive depth profile, i.e. they represent the temperature of the re-equilibration between the water film and the rock mass a short distance above the point of measurement. Here, we hypothesize that the magnitude of the convective signature is a function of the film advection rate (v_f proportional to the drip rate), the film thickness (b) and the flow distance (L). Baker et al. (2014) measured the thickness of water films on speleothems and found a dependency on the curvature and roughness of its surface. Considering the number of unknowns and the fact that convective and conductive heat transport are both contributing during film flow, it is highly challenging to predict the water temperature as a function of distance.

As can be seen in the long-term drip water temperature record (Fig. 6), film heat convection is initiated at the onset of drip events. However, it is most pronounced at the times with a large (exponential) temperature–depth gradient along the profile. This thermal gradient is caused by the conduction of the annual temperature signal into the subsurface rock mass. Consequently, the thermal effect of convection on drip water is a pronounced heating after summer and cooling after winter solstice. Further, it is most muted around the equinoxes due to a reversing temperature–depth profile. Importantly, any convective influence on drip water temperature caused by *film advection along cave walls* will be muted at depths beyond the reach of the annual harmonic signal (see discussion further below).

4.1.1.3. Exchange of moisture (m_{atm}) and thermal energy ($q_{f,atm}$) between surface and cave

When caves are open to the atmosphere air is exchanged (Conn, 1966), with the “chimney effect” (caused by an unstable density difference) being a common cause of venting (i.e., De Freitas et al., 1982; Oh and Kim, 2011). Here we observe that the surface air is frequently denser than the shallow cave air during summer (Fig. 7C) and continuously during winter (Fig. 7F) which causes Cathedral Cave to be a well vented cave. At this point the question arises: How deep do venting events propagate into the cave?

Cuthbert et al. (2014a) have shown that the drip water temperatures at a continuous slow drip source located ~40 m into the cave (site B) was continuously ~0.6 °C cooler than the surrounding speleothem and air temperature, at a depth where conduction of heat from the surface is muted and where RH values are stable at ~92%. Further, evaporation rates measured at different locations increasingly deeper in the cave show that the venting effect must dampen with distance from entry, which is consistent with

observations in other caves (Perrier et al., 2010; Faimon et al., 2012). However, despite the fact that the high frequency venting events do not directly show up at site C (Fig. 1) a potential for evaporation does exist since the RH is ~97%. Maintaining RH at less than saturation would not be possible without air exchange and, thus, drier and denser surface air must continuously replace moist and lighter air from deep within the cave.

Our findings are consistent with those from Buecher (1999) who reported a significant moisture loss at an average cave RH of 99.4% due to venting in Kartchner Caverns located in semi-arid Arizona. While cave venting has previously been investigated (Smithson, 1991; Tarhule-Lips and Ford, 1998; Spotl et al., 2005) and its effects on the moisture loss have been analysed (McLean, 1971; Buecher, 1999; De Freitas and Schmekal, 2003), we emphasize that potentially significant amounts of thermal energy in the form of latent heat continuously leaves the cave in the form of water vapour. This raises the question whether ongoing evaporation and associated cooling can significantly lower the overall temperatures of caves as well as individual drips? This could be answered by quantifying the energy lost through latent heat as a fraction of the total cave energy balance.

4.1.2. Conductive heat transport

4.1.2.1. Conduction of the surface temperature signal into the subsurface ($q_{c,atm}$)

Conduction of surface air temperature signals into the subsurface is a well-accepted phenomenon (Smerdon et al., 2003, 2004). Table 4 shows that the depth propagation of the annual harmonic through rock mass complies well with the theory (Equation (1)). Dominguez-Villar et al. (2013) made use of cave thermal anomalies, measured in the cave air, to infer that vegetation change at the surface influenced subsurface conduction. Further, the signature of global warming was found in cave air temperature data at a depth of 37 m (Dominguez-Villar et al., 2014). We present 2 years of surface air temperature and cave air measurements, as well as 1 year of speleothem, water film and drip water temperatures at different depths along a flow profile. We illustrate that Equation (1) is able to predict the subsurface penetration of the annual harmonic component by conduction from the ground surface temperature signal considering multiple layers with different thermal properties. This should equally apply to any other harmonic contained in the surface temperature signal as long as it is of sufficient magnitude and duration not to be damped beyond detectability.

The data shown in Figs. 3 and 6 demonstrate that the penetration of the annual temperature variation controls the drip water temperature at site A. The surface temperature signal generates the “background” temperature for drip water, but with exponentially damped amplitude and linearly shifted phase proportional with depth. Here, the differences in mean annual temperature can be explained with temperature changes that are slower than annual.

4.1.2.2. Conduction between speleothem and water film ($q_{c,rock}$)

The mechanism of heat conduction between speleothem and the water film, albeit “smeared” by convection, is evident from the drip water temperatures measured during both irrigation experiments (Figs. 4A and 5A). The first irrigation experiment (cooled water was applied to the surface on three consecutive days, Fig. 5) clearly illustrated that the pre-existing temperature–depth gradient (the subsurface temperature decreases exponentially with depth in summer) warmed the infiltrating colder irrigation water by conduction to produce the arrival of warm pulses on the speleothem at the onset of dripping (Fig. 5B). The time it took for the deuteriated water to arrive at the drip source (Fig. 5C) indicates a relatively long residence time of water in the epikarst stores (~48 h), for relatively

large volumes of water applied and an extreme temperature difference between water and rock. This demonstrates that any temperature disequilibrium between rock and water from location b onwards (Fig. 2) must have originated from the subsurface rock mass. During irrigation experiment 2 similar increases in the water temperature were observed after dripping had started. Therefore, the increase in drip temperature after flow started was caused by conduction from the warmer speleothem to the water further upstream of the profile (exponentially decreasing rock temperature with depth in summer), followed by convective heat transfer due to film advection, and subsequent conduction from the warmer water film back into the rock further downstream (Cuthbert et al., 2014a).

The fact that the relative magnitude of the warming anomaly remained the same for sensors located further along the profile is evidence for conduction between water film and rock (Fig. 4A). The amount of thermal energy conducted depends on the time that the water film is in contact with a particular area of speleothem, the film thickness (b) and the temperature difference. The contact time is determined by the velocity of the film flow (v_f), which is proportional to the drip rate measured. There is a slow temperature tailing of the water film and drip temperature (Fig. 4A) in all records along the flow stone (L). This is caused by conduction of thermal energy from the warmer water film back into the cooler speleothem when convection becomes less significant than conduction at decreasing film advection (= drip rates).

The temperature sensors that were inserted 4 cm into the speleothem confirm that the thermal anomaly caused by the flowing water film is transferred into the speleothem. These sensors show a temperature damping and lag with distance into the speleothem that is characteristic of heat conduction (red lines in Fig. 4A). Below a certain film advection rate (~20 drips/min in this case), convective warming ceases to dominate and is overwhelmed by evaporative cooling (the cross-over of lines e & f in Fig. 4A) illustrating that there is a temporary thermal equilibrium (Fig. 4A). Consequently, if the water film advection rate is sufficiently slow or the film is thin enough the drip water temperature is controlled by the speleothem temperature but only in the absence of impacts from cave climate (i.e. evaporative cooling).

4.1.2.3. Conduction between air and water film or rock wall ($q_{c,air}$)

The cave air shows a vertical temperature gradient that is similar to the subsurface rock temperature gradient under stable conditions, i.e. no flow and no venting events (Fig. 4A). Thermal anomalies can propagate much quicker through air than rock or water because the thermal diffusivity of air is approx. 22 and 146 times larger than that of the rock and water, respectively (Table 2). However, the heat capacity of air is in excess of ~4000 and ~2500 times smaller than water and rock, respectively. This means that the energy contained in thermal anomalies brought into the cave by air venting is effectively damped by the rock (Perrier et al., 2010). Nevertheless, an example of heat conduction between air and drip water can be seen during irrigation experiment 1: A venting event transports cooler air from the atmosphere into the cave temporarily lowering the temperature of the drip source by ~1 °C (grey arrow in Fig. 5A). The drip had ceased to be active at the time however the speleothem surface was still wet.

During winter the cave is continuously vented and the cave air temperature fluctuates periodically with varying amplitudes that depend on the surface climate (Fig. 7E). This thermal signature is almost exactly replicated by the drip source temperature showing the mechanism of conduction between air and speleothem or air and water film (Fig. 7D). The magnitude of temperature variation depends on the magnitude of air flow which is proportional to the air density difference (Faimon et al., 2012).

4.1.3. Latent heat and mass transport

4.1.3.1. Latent heat ($q_{l,air}$) and mass (m_{air}) exchange between the water film and cave air

Cuthbert et al. (2014a) previously demonstrated evaporative cooling of speleothem drip water, by as much as $-1.5\text{ }^{\circ}\text{C}$ compared to the cave air temperature. We have shown in new data presented here that this may be as high as $-2.5\text{ }^{\circ}\text{C}$ (Fig. 5). This anomaly was not caused by heat convection due to subsurface water percolation transporting the cooled irrigation water via preferential or fracture flow between surface and cave, as deuterium breakthrough had not yet occurred (Fig. 5C). The cooling occurred because the previously dry flowstone surface was wetted by the drip response to surface irrigation. In fact, at one location (k2 in Fig. 5B) cooling of the wet flowstone to below air temperature continued after film flow had ceased. As the absence of dripping (and therefore film flow) rules out the possibility of convective cooling from cooled irrigation water applied to the surface, the cooling anomaly must be caused by evaporation.

In Fig. 6 we present a new longer record of temperatures measured on 3 points along the speleothem surface including drip source (stalactite). It is obvious that frequent evaporative cooling events (Fig. 7A) are directly coupled to venting events lowering the RH during summer (Fig. 7C). Without venting the cave air RH would reach saturation over time and diminish the potential for evaporation. While Buecher (1999) found that cave evaporation rates are very sensitive to changes in RH, we observe that the vapour deficit also directly influences the magnitude of evaporative drip water cooling (Figs. 4 and 7A–C).

From results presented here it is clear that air venting causes a complex thermodynamic coupling of cave and surface climate that influences the cave drip water temperature. We illustrate frequent and significant evaporative cooling and associated moisture exchange between drip water and cave air caused by frequent exchange of humid cave air with dry surface air. Dreybrodt et al. (2005) reported that cave walls can be warmed due to the release of latent heat during condensation in caves located in a humid climate. While our results show that in-cave evaporation can cause cooling, we anticipate that condensation could warm cave drip water. We illustrate that, when venting is present, cave drip water temperature near cave entrances can contain significant diurnal fluctuations or continuous cooling relative to cave air whenever RH is below a certain threshold. However, for drip water temperature to be affected by the cave climate it must be exposed to the cave air for some time before arriving at the drip source, e.g. as a water film flowing over speleothem surfaces such as flowstones, stalactites and draperies.

4.2. Implications for speleothem-based paleoclimate reconstructions

4.2.1. Relationship between temperature at the surface and drip source

Drip water temperature is a key variable to be considered when the paleoclimate records are reconstructed from speleothem archives. Current methods allow for paleo-temperature reconstruction (i.e. from $\delta^{18}\text{O}$) with seasonal and even monthly resolution (i.e., Treble et al., 2007; Orland et al., 2009). The spatial resolution of speleothem milling, and therefore the temporal resolution of climate proxies, is likely to increase in the future with the development of better technologies. While the surface temperature is typically the result of interest, many geochemical proxies depend on the temperature of the water at the drip source. This necessitates a better understanding of processes affecting the temperature at the surface of the speleothem at the time of its formation. Past

surface climate estimates can be influenced by assumptions about the conditions along the flow path between surface and drip source.

Our results demonstrate that, in the absence of cave venting and convective thermal breakthrough from the surface, the drip water temperature is primarily a function of subsurface heat conduction, i.e. infiltrating surface water is quickly equilibrated to the subsurface temperature–depth profile. A universally applicable model to describe the relationship between surface and drip water temperature in this case is the differential equation for conductive heat transport (Carslaw and Jaeger, 1959). It is important to note that thermal modelling requires subsurface thermal parameters such as presented in Table 2. However, these are in general reasonably well constrained and references to suitable literature can be found in Rau et al. (2014). While significant temperature anomalies due to convective heat transport from the surface that could imprint on paleoclimate proxies can be ruled out in our case, we note that this could be possible under different karst settings. However, we expect the likelihood of such temperature anomalies to decrease with increasing subsurface depth.

The presence of the annual temperature signal in our data (Fig. 3) facilitated the use of an analytical solution that is based on a harmonic temperature input at the surface (Equation (1)). While this solution is useful for estimating the subsurface temperature response to cyclic drivers (e.g. annual, decadal, centennial or millennial), many paleoclimate events of interest are based on non-cyclic changes in the surface temperature, e.g. rapid climate change (Holmes et al., 2011). Modelling the latter would require the selection of a suitable model to quantify the temperature evolution between surface and drip source. For example, the analytical solution used by Domínguez-Villar et al. (2013) describes the subsurface temperature as a function of depth and time based on a step change in surface temperature. Drip source temperature signals can be predicted from arbitrary surface temperature–time signals using a time convolution of this model. Vice versa, a deconvolution can unravel the surface temperature from a speleothem-based paleoclimate proxy.

4.2.2. Optimising the speleothem sampling location

Our measurements show that drip water temperature is controlled by a complex thermal coupling between the subsurface rock background temperature driven by the ground surface temperature and the cave climate driven by ventilation. This requires careful consideration when deciding speleothem sampling locations. For example, the stalactite on which the drip temperature was measured (Fig. 2A–B) was exposed to an annual temperature variation of $\sim 5.21\text{ }^{\circ}\text{C}$ as conducted from the surface but with a delay of ~ 2.6 months (80 days) compared to the surface temperature signal. This is a significant variation when the temperature dependency of speleothem growth is considered (Hendy, 1971; Casteel and Banner, 2015) and if seasonal surface temperature is to be reconstructed.

Fig. 9 shows the propagation of selected frequency components with an average soil zone thickness of 0.1 m and an underlying epikarst to a depth of 100 m as a generic example but also resembles the Cathedral Cave setting. Calculations are based on the laboratory measurements of thermal parameters. Envelopes for minimum and maximum thermal diffusivity for soil and bedrock as reported in the literature (Table 2) were also determined for transferability of the results, i.e. when different materials are present at different field sites. Fig. 9 clearly illustrates the characteristic amplitude damping and phase shifting with depth, inherent to the different harmonic signals. For example, it might be useful for a researcher to maximise or minimise the annual temperature signal (which may determine the presence of annual geochemical

laminae useful for chronology building) compared to the long-term paleoclimate signal. If a speleothem location was to be selected where the maximum annual temperature variation should not be larger than 1 °C (0.5 °C amplitude) the surface amplitude damping factor is ~ 0.059 (0.5 °C/8.51 °C). In the absence of venting and convective heat transport through preferential or fracture flow, the desired variation is not exceeded at total depths of greater than ~ 8.6 m (red dot in Fig. 9A).

Another important consideration, when paleoclimate is to be inferred from speleothem archives, is the phase shift. Again an example close to our case: A surface temperature signal with centennial period is shifted by ~ 7.82 years (94 months) at 15 m depth (red dot in Fig. 9B). Hence, this should be taken into account either when an accurate resolution of temporal (i.e. seasonal) climate patterns is desired or when climatic patterns are compared to other sources of information. Table 5 exemplifies minimum and maximum expected damping factors and signal shifts for distinct depths extracted from Fig. 9. This lag is within resolution of long-record dating (Cheng et al., 2009) and could explain previous lag times between drip source related signals and surface events (Domínguez-Villar et al., 2009).

The above discussion illustrates that the speleothem sampling location will not only depend on the type of proxy (i.e., $\delta^{18}\text{O}$, $\delta^{13}\text{C}$, Δ_{47} , trace metals, organics) but also on what archived harmonic signal resolution is desired. The increasing temporal resolution for drip source temperature dependent proxies makes shallow sampling attractive to maximise the high frequency temperature signal (i.e., seasonal to annual). However, near-entrance locations require a good quantitative understanding on the influence from cave climate, such as evaporation (or condensation) discussed below. Deep samples are better for long-term surface dependent proxies as higher frequency temperature harmonics are essentially damped out. Equations (1) and (2), as visualised in Fig. 9 and Table 5, can serve as a guide for targeted speleothem sampling.

4.2.3. Cave venting and evaporation

As a further point of discussion we illustrate that cave venting, besides influencing pCO_2 (Spotl et al., 2005; Baldini et al., 2008; Kowalczyk and Froelich, 2010), can alter cave drip water temperature and consequently influence speleothem growth. In fact, Casteel and Banner (2015) illustrate that seasonal temperature variations control calcite growth rates and trace element ratios. We

emphasise that significant and frequent in-cave evaporation and drip water cooling is to be expected for near-entrance parts of caves that are located in present (or past) low humidity environments. Fig. 10 summarises the evaporative cooling potential at Cathedral Cave. While there is a weak correlation between drip water cooling and RH the data exhibits significant scattering which indicates that additional parameters affect the cooling, e.g. flow path, drip rate and air circulation. We observed up to -1.8 °C at a RH of $<95\%$ for drip water that is exposed to the cave air. Unravelling the dependency of drip water evaporative cooling on venting clearly requires further research.

While we illustrate that evaporative drip water cooling is caused by regular ingress of dry air during summer (Fig. 7A–C), in-cave evaporation also occurs during winter as the outside air is permanently denser (Fig. 7D–F). Our results prove that Cathedral Cave is well vented near the entrance despite the lack of discernible air movement. Results also indicate that moisture escapes from even the deepest parts of the cave (RH $< 100\%$, evaporation rate > 0 mm) but measurable influences on the drip water temperature were not detected.

It is well accepted that venting influences geochemical signatures (Spotl et al., 2005; Baldini et al., 2008). We point out that evaporation leads to isotopic enrichment of drip water (Cuthbert et al., 2014b; Markowska et al., submitted for publication), and that evaporative drip water cooling could significantly influence chemical/isotopic signatures in speleothems (Kim and O'Neil, 1997). This may be a further complication in reconciling clumped isotope thermometry Δ_{47} based temperature proxies in speleothems with mean air temperature, as Δ_{47} will be affected by the temperature of the water film from which the carbonate is precipitated (Affek et al., 2008).

Our results are consistent with Perrier et al. (2010) in that ventilation related effects, such as evaporation and associated cave rock and drip water temperature anomalies, are damped with increasing distance from the entrance. However, the magnitude of venting will strongly depend on the cave geomorphology (De Freitas et al., 1982). In fact considerable air flow has been reported within caves (Conn, 1966; McLean, 1971; Cigna and Forti, 1986), in particular when multiple entries located at different vertical elevations are present (Faimon et al., 2012; Gregoric et al., 2013). Fig. 10 presents the first quantification of the effects of evaporative cooling of cave drip water. Our data is just from two drip sites in one cave, and further empirical field data is needed to

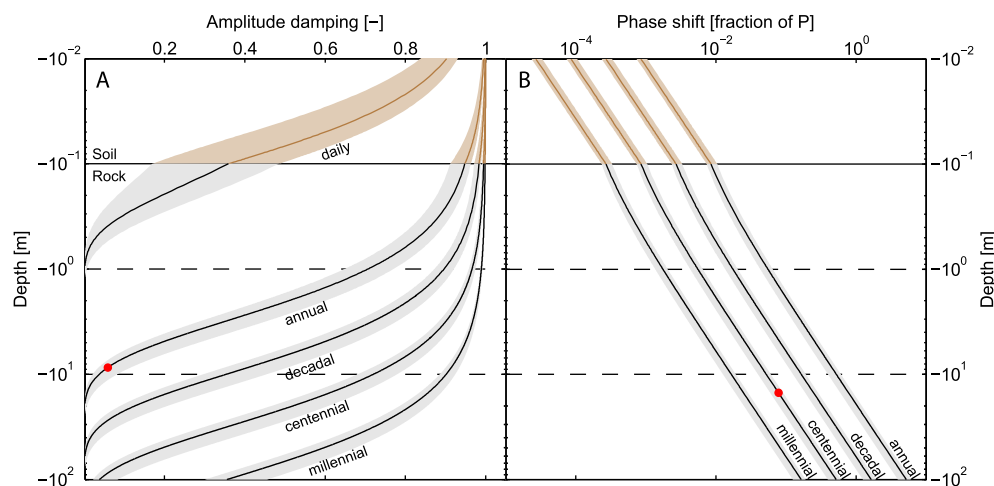


Fig. 9. Depth penetration of surface temperature components based on Equations (1) and (2) and thermal parameters in Table 2 with selected frequencies (daily, annual, decadal, centennial and millennial): A) amplitude damping, B) phase shift. The grey bands enveloping the curves reflect the variability arising from min/max thermal parameters reported in the literature. The red dots illustrate practical examples given in the discussion.

Table 5
Max/min damping factors (ratio between subsurface and surface amplitude) and signal shifts for distinct depths and different harmonic signals extracted from Fig. 9.

Harmonic		Daily		Annual		Decadal		Centennial		Millennial	
Depth [m]		Min	Max	Min	Max	Min	Max	Min	Max	Min	Max
0.1	Amp [–]	0.17	0.49	0.91	0.96	0.97	0.99	0.99	1.00	1.00	1.00
	Phase [months]	0.0	0.0	0.1	0.1	0.3	0.4	0.9	1.3	2.8	4.0
1	Amp [–]	0	0.01	0.65	0.77	0.87	0.92	0.96	0.97	0.99	1.00
	Phase [months]	–	–	0.5	0.8	1.6	2.5	5.1	7.8	16.3	24.5
10	Amp [–]	0	0	0.02	0.08	0.30	0.46	0.68	0.78	0.89	0.92
	Phase [months]	–	–	4.8	7.3	15.1	23.0	47.8	72.8	151.0	230.3
100	Amp [–]	0	0	0	0	0	0	0.02	0.08	0.30	0.46
	Phase [months]	–	–	–	–	–	–	473	723	1498	2288

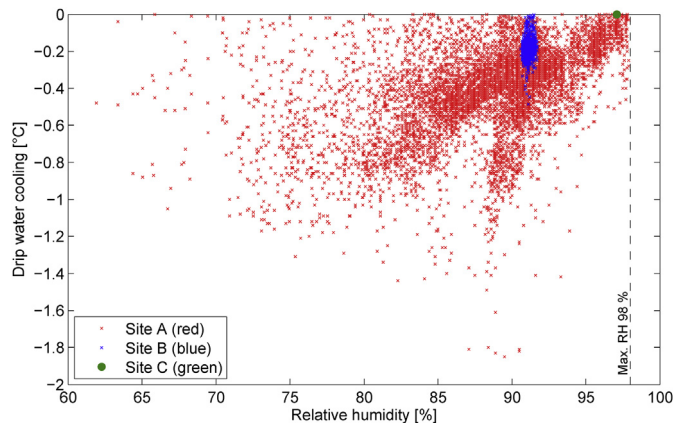


Fig. 10. The evaporative cooling potential: difference between cave air and drip water temperature plotted against RH. Site A: ~2 months of summer data (Fig. 6). Site B: Data from the irrigation experiment 2 (Fig. 3B in Cuthbert et al., 2014a). Site C: ~4 months of measurements.

develop a predictive model of factors determining the extent of evaporative cooling. However, the implications for speleothem temperature proxies are clear – in ventilated caves, researchers should consider the possibility that the speleothem proxy temperature is systematically cooler than the external mean air temperature.

4.2.4. Considerations for the type of speleothem to be sampled

A question arises as a result of the above discussion: What type of speleothem should be sampled to best constrain the drip water temperature? Site 1 has a stalagmite fed from a flowstone with a relatively long path (~3 m) where the water is exposed to the cave atmosphere via film flow. While we expect this type of speleothem would have a large potential for thermal disequilibrium affecting temperature proxies, it could still be a good source for soil or vegetation derived signals (i.e., pollen). A stalagmite fed by a regular conical-shaped stalactite will have drip water flowing along the outside of the deposit. This type of speleothem would be cooled during periods when the drip rate is slow and regular (Cuthbert et al., 2014a) which may imprint on the geochemical proxy and make interpretation difficult. We believe that the best stalagmite (likely a candlestick shape) for sampling is fed by a soda-straw stalactite because the flow path to the drip is surrounded by (thin) calcite and the water is therefore less exposed to the cave atmosphere and potential evaporative cooling. However, confirming this requires further research.

4.2.5. Summary

The implications of our results for speleothem paleoclimate reconstruction can be summarised as follows:

- The location that the proxy-derived temperature signal is representative for (i.e., surface or drip source) and the processes that could influence the signal must be carefully considered. Depending on the requirements, Equation (1) offers a quantitative model to convolve or deconvolve the “background” temperature signal between surface and drip source onto which in-cave signals will be superimposed.
- The damping of surface temperature variations in the soil/epikarst is a function of subsurface depth and frequency (Fig. 9). If a surface temperature signal is required as a paleoclimate proxy (i.e., a decadal-scale temperature signal) a near-surface chamber, again with minimum venting and maximum relative humidity, should fulfil the conditions for sampling.
- Fig. 9 illustrates the importance of considering the subsurface depth when speleothems are sampled for the purpose of accurately unravelling the surface temperature signal from isotope proxies. For example, highest amplitudes for the surface temperature during glacial–interglacial climate transitions and for the variability over the last 10,000 years are 5 °C and 0.5–1 °C, respectively (Cheng et al., 2009). A rough guide for selecting appropriate sampling depths where the desired signal can be resolved is given in Table 5.
- We stress that, consistent with the results of Cuthbert et al. (2014a), frequent evaporative cooling events are to be expected in caves that could have been ventilated or exposed to evaporation (RH < 100%). Evaporative cooling can lower the drip water temperature compared to cave air/speleothem temperature. The best cave locations to minimise this effect are those with a long-term RH of 100% and no air flow. These criteria were set out in the 1960s to determine where to best sample speleothems for temperature records from ¹⁸O (Hendy, 1971). Here we show that, while the premise was correct, correction of the temperature signal should be considered. The influence could be assessed by checking for a difference in air and drip water temperature.
- The best speleothems to sample and analyse to obtain paleoclimate records of surface air temperature changes are minimum diameter stalagmites that are supplied by soda-straw stalactites. While the speleothem–water contact is maximised over water–air contact, the drip rates for these specimens are likely to be slow and evaporation could still occur, and therefore caves of RH of 100% and no air flow would provide ideal sampling locations.

5. Conclusion

Cave drip water temperature is controlled by multiple heat transfer mechanisms acting simultaneously during the movement of water through soil and bedrock and as film flow over speleothem surfaces, i.e. conduction, convection and latent heat and mass exchange. The two main heat sources/sinks are: 1) conduction of the

dynamic surface temperature signal vertically into the subsurface, 2) the cave atmosphere as is coupled to the surface atmosphere by different venting mechanisms. The relative importance of each mechanism depends on the thickness of the overburden, the distance of film flow between entering the cave and the arriving at the drip source, and the advective velocity of the water film which is proportional to the drip rate.

While cave air temperatures have been measured and analysed in detail, there is a general lack of data and understanding relating to controls of cave drip water temperature. We deployed multiple specialised high-resolution sensors along an in-cave flow path and drip source to measure the evolution of the speleothem/water temperature. In-cave dripping was induced through manual surface irrigation experiments with cooled water and deuterium as a conservative tracer. In combination with measurements of drip rates, surface and cave climate, in-cave evaporation rates and deuterium concentrations we identified and analysed, for the first time, the heat transfer processes that exert control on the cave drip water temperature between surface and drip source.

Temperature harmonics contained in the surface temperature signal propagate conductively into the subsurface and undergo frequency dependent exponential amplitude damping and linear phase shifting with subsurface depth. For example, we observed that there is a clear exponential temperature–depth gradient induced by the annual surface temperature harmonic which controls the drip water temperature (“background” temperature). Film flow along the speleothem surface can convectively carry this signal down along the flow path causing temperature anomalies that depend on the film advection rate (which is proportional to the drip rate). However, this convective temperature anomaly is damped (“smeared”) by conduction back into the speleothem along the flow path depending on the temperature–depth gradient at the time.

At the same time the water film is exposed to the cave air which can significantly change drip water temperature through convection/conduction or latent heat and mass exchange, with magnitudes that depend on the distance from the cave entrance. The influence on the water temperature, however, depends on the film advection rate and the complex coupling between surface and cave climate through venting (i.e. air exchange induced by a density difference between surface and cave air). We observed regular evaporative drip water cooling events of $-1.5\text{ }^{\circ}\text{C}$ and up to $-2.5\text{ }^{\circ}\text{C}$ during summer when denser low-RH air enters the cave. Further, the drip water temperature can also fluctuate due to air-induced convection/conduction in winter when surface air is continuously denser (constant venting).

Drip water temperature is a key parameter controlling many biogeochemical in-cave processes that must be quantified when the paleoclimate is reconstructed from speleothem-based archives. We advise how the drip water “background” temperature can be modelled using simple analytical solutions of the differential heat conduction equation. We show how a data supported conceptual model for cave drip water temperature can assist with constraining a range of temperature sensitive biogeochemical speleothem processes. Further, we offer guidance on the type and location of speleothems that are sampled for paleoclimate signals with the intent to either maximise or minimise the drip water temperature signature. We anticipate that our findings will lead to significant improvements in the understanding of climate signals from speleothem based paleoclimate archives.

Acknowledgements

Funding for this research was provided by the National Centre for Groundwater Research and Training, an Australian Government initiative, supported by the Australian Research Council and

the National Water Commission (Grant SRI2009R1). Funding was also provided by the Gary Johnston fund that started the Chair of Water Management at UNSW. Mark Cuthbert was supported by Marie Curie Research Fellowship funding from the European Community's Seventh Framework Programme [FP7/2007-2013] under grant agreement n.299091. The climate station, Stalagmites and the specialised temperature monitoring equipment were provided by the Australian Government National Collaborative Research Infrastructure Strategy (NCRIS). We thank: Evan Jensen, Chris George, Col Birchall, Mike Augée and Eliza Wells for practical and logistical support during the irrigation experiments; Bruce Welsh and Philip Maynard from Sydney University Speleological Society for the cave survey map; Mark Whelan for help designing and building the high-resolution temperature equipment; Paul Brockbank from the School of Chemical Engineering workshop for his precision in drilling holes into a limestone sample so that thermal measurements could be conducted. The manuscript was significantly improved thanks to feedback from Claude Hillaire-Marcel (editor), Corinne Wong (guest editor) and an anonymous reviewer.

References

- Affek, H.P., Bar-Matthews, M., Ayalon, A., Matthews, A., Eiler, J.M., 2008. Glacial/interglacial temperature variations in Soreq cave speleothems as recorded by ‘clumped isotope’ thermometry. *Geochim. Cosmochim. Acta* 72, 5351–5360. <http://dx.doi.org/10.1016/j.gca.2008.06.031>.
- Atkinson, T., Smart, P., Wigley, T., 1983. Climate and natural radon levels in Castleguard cave, Columbia Icefields, Alberta, Canada. *Arct. Alp. Res.* 487–502.
- Baker, A., Genty, D., Dreybrodt, W., Barnes, W.L., Mockler, N.J., Grapes, J., 1998. Testing theoretically predicted stalagmite growth rate with recent annually laminated samples: implications for past stalagmite deposition. *Geochim. Cosmochim. Acta* 62, 393–404.
- Baker, A.J., Matthey, D.P., Baldini, J.U.L., 2014. Reconstructing modern stalagmite growth from cave monitoring, local meteorology, and experimental measurements of dripwater films. *Earth Planet. Sci. Lett.* 392, 239–249. <http://dx.doi.org/10.1016/j.epsl.2014.02.036>.
- Baker, D.G., Ruschy, D.L., 1993. The recent warming in eastern Minnesota shown by ground temperatures. *Geophys. Res. Lett.* 20, 371–374.
- Baldini, J.U., McDermott, F., Hoffmann, D.L., Richards, D.A., Clipson, N., 2008. Very high-frequency and seasonal cave atmosphere pCO₂ variability: implications for stalagmite growth and oxygen isotope-based paleoclimate records. *Earth Planet. Sci. Lett.* 272, 118–129.
- Bendjoudi, H., Cheviron, B., Guérin, R., Tabbagh, A., 2005. Determination of upward/downward groundwater fluxes using transient variations of soil profile temperature: test of the method with Voyons (Aube, France) experimental data. *Hydro. Process.* 19, 3735–3745.
- BOM, 2014. Climate Statistics for Australian Locations: Wellington (Agrowplow). Bureau of Meteorology, Australian Government. http://www.bom.gov.au/climate/averages/tables/cw_065034_All.shtml (accessed Dec 2014).
- Buecher, R.H., 1999. Microclimate study of Kartchner caverns, Arizona. *J. Cave Karst Stud.* 61, 108–120.
- Carlslaw, H.S., Jaeger, J.C., 1959. *Conduction of Heat in Solids*, second ed. Clarendon Press, Oxford.
- Camporeale, C., Ridolfi, L., 2012. Hydrodynamic-driven stability analysis of morphological patterns on stalactites and implications for cave paleoflow reconstructions. *Phys. Rev. Lett.* 108, 238501.
- Casteel, R.C., Banner, J.L., 2015. Temperature-driven seasonal calcite growth and drip water trace element variations in a well-ventilated Texas cave: Implications for speleothem paleoclimate studies. *Chem. Geol.* 392, 43–58.
- Cheng, H., Edwards, R.L., Broecker, W.S., Denton, G.H., Kong, X., Wang, Y., Zhang, R., Wang, X., 2009. Ice Age terminations. *Science* 326, 248–252. <http://dx.doi.org/10.1126/science.1177840>.
- Cheviron, B., Guérin, R., Tabbagh, A., Bendjoudi, H., 2005. Determining long-term effective groundwater recharge by analyzing vertical soil temperature profiles at meteorological stations. *Water Resour. Res.* 41.
- Clauser, C., Huenges, E., 1995. Thermal conductivity of rocks and minerals. In: *Rock Physics and Phase Relations: A Handbook of Physical Constants*, vol. 3, pp. 105–126. <http://dx.doi.org/10.1029/RF003p0105>.
- Conn, H.W., 1966. Barometric wind in wind and jewel caves, South Dakota. *Natl. Speleol. Soc. Bull.* 28, 55–69.
- Covington, M.D., Luhmann, A.J., Gabrovšek, F., Saar, M.O., Wicks, C.M., 2011. Mechanisms of heat exchange between water and rock in karst conduits. *Water Resour. Res.* 47, W10514. <http://dx.doi.org/10.1029/2011WR010683>.
- Covington, M.D., Luhmann, A.J., Wicks, C.M., Saar, M.O., 2012. Process length scales and longitudinal damping in karst conduits. *J. Geophys. Res. Earth Surf.* 117, F01025. <http://dx.doi.org/10.1029/2011JF002212>.

- Cuthbert, M.O., Baker, A., Jex, C.N., Graham, P.W., Treble, P.C., Andersen, M.S., Ian Acworth, R., 2014b. Drip water isotopes in semi-arid karst: implications for speleothem paleoclimatology. *Earth Planet. Sci. Lett.* 395, 194–204.
- Cuthbert, M.O., Rau, G.C., Andersen, M.S., Roshan, H., Rutledge, H., Marjo, C.E., Markowska, M., Jex, C.N., Graham, P.W., Mariethoz, G., Acworth, R.I., Baker, A., 2014a. Evaporative cooling of speleothem drip water. *Sci. Rep.* 4 <http://dx.doi.org/10.1038/srep05162>.
- De Freitas, C., Littlejohn, R., Clarkson, T., Kristament, I., 1982. Cave climate: assessment of airflow and ventilation. *J. Climatol.* 2, 383–397.
- De Freitas, C., Littlejohn, R., 1987. Cave climate: assessment of heat and moisture exchange. *J. Climatol.* 7, 553–569.
- De Freitas, C., Schmekel, A., 2003. Condensation as a microclimate process: measurement, numerical simulation and prediction in the Glowworm cave, New Zealand. *Int. J. Climatol.* 23, 557–575.
- De Vries, D.A., 1963. Thermal properties of soils. *Physics of Plant Environment*.
- Dominguez-Villar, D., Fairchild, I.J., Baker, A., Carrasco, R.M., Pedraza, J., 2013. Reconstruction of cave air temperature based on surface atmosphere temperature and vegetation changes: implications for speleothem palaeoclimate records. *Earth Planet. Sci. Lett.* 369, 158–168.
- Dominguez-Villar, D., Fairchild, I.J., Baker, A., Wang, X., Edwards, R.L., Cheng, H., 2009. Oxygen isotope precipitation anomaly in the North Atlantic region during the 8.2 ka event. *Geology* 37, 1095–1098. <http://dx.doi.org/10.1130/g30393a.1>.
- Dominguez-Villar, D., Lojen, S., Krklec, K., Baker, A., Fairchild, I.J., 2014. Is global warming affecting cave temperatures? Experimental and model data from a paradigmatic case study. *Clim. Dyn.* 1–13.
- Dreybrodt, W., 1981. The kinetics of calcite precipitation from thin films of calcareous solutions and the growth of speleothems: revisited. *Chem. Geol.* 32, 237–245.
- Dreybrodt, W., Gabrovšek, F., Perne, M., 2005. Condensation corrosion: a theoretical approach. *Speleogenes. Evol. Karst Aquifers* 3.
- Epstein, S., Buchsbaum, R., Lowenstam, H.A., Urey, H.C., 1953. Revised carbonate-water isotopic temperature scale. *Geol. Soc. Am. Bull.* 64, 1315–1326.
- Faimon, J., Troppová, D., Baldík, V., Novotný, R., 2012. Air circulation and its impact on microclimatic variables in the Císařská Cave (Moravian Karst, Czech Republic). *Int. J. Climatol.* 32, 599–623.
- Giacomo, P., 1982. Equation for the determination of the density of moist air (1981). *Metrologia* 18, 33.
- Goto, S., Yamano, M., Kinoshita, M., 2005. Thermal response of sediment with vertical fluid flow to periodic temperature variation at the surface. *J. Geophys. Res. Sol. Earth* 110, B01106.
- Hendy, C.H., 1971. The isotopic geochemistry of speleothems—I. The calculation of the effects of different modes of formation on the isotopic composition of speleothems and their applicability as palaeoclimatic indicators. *Geochim. Cosmochim. Acta* 35, 801–824. [http://dx.doi.org/10.1016/0016-7037\(71\)90127-X](http://dx.doi.org/10.1016/0016-7037(71)90127-X).
- Holmes, J., Lowe, J., Wolff, E., Srokosz, M., 2011. Rapid climate change: lessons from the recent geological past. *Glob. Planet. Change* 79, 157–162. <http://dx.doi.org/10.1016/j.gloplacha.2010.10.005>.
- Horai, K.-I., 1971. Thermal conductivity of rock-forming minerals. *J. Geophys. Res.* 76, 1278–1308. <http://dx.doi.org/10.1029/JB076i005p01278>.
- Jex, C.N., Mariethoz, G., Baker, A., Graham, P., Andersen, M.S., Acworth, I., Edwards, N., Azcurra, C., 2012. Spatially dense drip hydrological monitoring and infiltration behaviour at the Wellington Caves, South East Australia. *Int. J. Speleol.* 41, 14.
- Kim, S.-T., O'Neil, J.R., 1997. Equilibrium and nonequilibrium oxygen isotope effects in synthetic carbonates. *Geochim. Cosmochim. Acta* 61, 3461–3475. [http://dx.doi.org/10.1016/S0016-7037\(97\)00169-5](http://dx.doi.org/10.1016/S0016-7037(97)00169-5).
- Kowalczyk, A.J., Froelich, P.N., 2010. Cave air ventilation and CO₂ outgassing by radon-222 modeling: how fast do caves breathe? *Earth Planet. Sci. Lett.* 289, 209–219.
- Luhmann, A.J., Covington, M.D., Myre, J.M., Perne, M., Jones, S.W., Alexander Jr., E.C., Saar, M.O., 2015. Thermal damping and retardation in karst conduits. *Hydrol. Earth Syst. Sci.* 19, 137–157. <http://dx.doi.org/10.5194/hess-19-137-2015>.
- Mariethoz, G., Baker, A., Sivakumar, B., Hartland, A., Graham, P., 2012. Chaos and irregularity in karst percolation. *Geophys. Res. Lett.* 39.
- Markowska, M., Baker, A., Andersen, M.S., Jex, C.N., Graham, P.W., Cuthbert, M.O., Rau, G.C., Rutledge, H., Mariethoz, G., Marjo, C.E., Treble, P.C., Edwards, N., 2015. It's all about evaporation: artificial and natural water isotope tracing in semi-arid karst. *Quat. Sci. Rev.* (submitted for publication).
- McLean, J.S., 1971. *The Microclimate in Carlsbad Caverns, New Mexico*. US Geological Survey, Albuquerque, New Mexico.
- NIST, 2014. NIST Chemistry WebBook. National Institute of Standards and Technology, U.S. Department of Commerce. <http://webbook.nist.gov/> (accessed Dec 2014).
- Northup, E., Lavoie, K.H.D., 2001. Geomicrobiology of caves: a review. *Geomicrobiol. J.* 18, 199–222.
- Ochsner, T.E., Horton, R., Ren, T., 2001. A new perspective on soil thermal properties. *Soil Sci. Soc. Am. J.* 65, 1641–1647. <http://dx.doi.org/10.2136/sssaj2001.1641>.
- Oh, Y.H., Kim, G., 2011. Factors controlling the air ventilation of a limestone cave revealed by 222Rn and 220Rn tracers. *Geosci. J.* 15, 115–119.
- Orland, I.J., Bar-Matthews, M., Kita, N.T., Ayalon, A., Matthews, A., Valley, J.W., 2009. Climate deterioration in the Eastern Mediterranean as revealed by ion microprobe analysis of a speleothem that grew from 2.2 to 0.9 ka in Soreq Cave, Israel. *Quat. Res.* 71, 27–35. <http://dx.doi.org/10.1016/j.yqres.2008.08.005>.
- Osborne, R., 2007. Cathedral Cave, Wellington Caves, New South Wales, Australia. A multiphase, non-fluvial cave. *Earth Surf. Process. Landf.* 32, 2075–2103.
- Perrier, F., Le Mouél, J.-L., Richon, P., 2010. Spatial and temporal dependence of temperature variations induced by atmospheric pressure variations in shallow underground cavities. *Pure Appl. Geophys.* 167, 253–276.
- Rau, G.C., Andersen, M.S., McCallum, A.M., Roshan, H., Acworth, R.I., 2014. Heat as a tracer to quantify water flow in near-surface sediments. *Earth Sci. Rev.* 129, 40–58.
- Rutledge, H., Baker, A., Marjo, C.E., Andersen, M.S., Graham, P.W., Cuthbert, M.O., Rau, G.C., Roshan, H., Markowska, M., Mariethoz, G., Jex, C.N., 2014. Dripwater organic matter and trace element geochemistry in a semi-arid karst environment: implications for speleothem paleoclimatology. *Geochim. Cosmochim. Acta* 135, 217–230. <http://dx.doi.org/10.1016/j.gca.2014.03.036>.
- Schärlü, U., Rybach, L., 2001. Determination of specific heat capacity on rock fragments. *Geothermics* 30, 93–110. [http://dx.doi.org/10.1016/S0375-6505\(00\)00035-3](http://dx.doi.org/10.1016/S0375-6505(00)00035-3).
- Schön, J.H., 1996. *Physical Properties of Rocks: Fundamentals and Principles of Petrophysics*, 583.
- Schouten, S., Woltering, M., Rijpstra, W.I.C., Sluijs, A., Brinkhuis, H., Sinninghe Damsté, J.S., 2007. The Paleocene–Eocene carbon isotope excursion in higher plant organic matter: differential fractionation of angiosperms and conifers in the Arctic. *Earth Planet. Sci. Lett.* 258, 581–592.
- Smerdon, J.E., Pollack, H.N., Cermak, V., Enz, J.W., Kresl, M., Safanda, J., Wehmiller, J.F., 2004. Air-ground temperature coupling and subsurface propagation of annual temperature signals. *J. Geophys. Res. Atmos.* (1984–2012) 109.
- Smerdon, J.E., Pollack, H.N., Enz, J.W., Lewis, M.J., 2003. Conduction-dominated heat transport of the annual temperature signal in soil. *J. Geophys. Res. Solid Earth* (1978–2012) 108.
- Smithson, P., 1991. Inter-relationships between cave and outside air temperatures. *Theor. Appl. Climatol.* 44, 65–73.
- Spötl, C., Fairchild, I.J., Tooth, A.F., 2005. Cave air control on dripwater geochemistry, Obir Caves (Austria): implications for speleothem deposition in dynamically ventilated caves. *Geochim. Cosmochim. Acta* 69, 2451–2468.
- Stallman, R.W., 1965. Steady One-Dimensional Fluid Flow in a Semi-Infinite Porous Medium with Sinusoidal Surface Temperature. *J. Geophys. Res.* 70, 2821–2827.
- Tabbagh, A., Bendjoudi, H., Benderitter, Y., 1999. Determination of recharge in unsaturated soils using temperature monitoring. *Water Resour. Res.* 35, 2439–2446.
- Taniguchi, M., 1993. Evaluation of vertical groundwater fluxes and thermal properties of aquifers based on transient temperature-depth profiles. *Water Resour. Res.* 29 (7), 2021–2026. <http://dx.doi.org/10.1029/93WR00541>.
- Taniguchi, M., Sharma, M.L., 1993. Determination of groundwater recharge using the change in soil temperature. *J. Hydrol.* 148, 219–229. [http://dx.doi.org/10.1016/0022-1694\(93\)90261-7](http://dx.doi.org/10.1016/0022-1694(93)90261-7).
- Tarhule-Lips, R.F., Ford, D.C., 1998. Condensation corrosion in caves on Cayman Brac and Isla de Mona. *J. Caves Karst Stud.* 60, 84–95.
- Tarnawski, V.R., Momose, T., Leong, W.H., 2011. Thermal conductivity of standard sands II. saturated conditions. *Int. J. Thermophys.* 32, 984–1005. <http://dx.doi.org/10.1007/s10765-011-0975-1>.
- Treble, P.C., Schmitt, A.K., Edwards, R.L., McKeegan, K.D., Harrison, T.M., Grove, M., Cheng, H., Wang, Y.J., 2007. High resolution secondary ionisation mass spectrometry (SIMS) $\delta^{18}\text{O}$ analyses of Hulu Cave speleothem at the time of Heinrich Event 1. *Chem. Geol.* 238, 197–212. <http://dx.doi.org/10.1016/j.chemgeo.2006.11.009>.
- Vosteen, H.-D., Schellschmidt, R., 2003. Influence of temperature on thermal conductivity, thermal capacity and thermal diffusivity for different types of rock. *Phys. Chem. Earth A/B/C* 28, 499–509. [http://dx.doi.org/10.1016/S1474-7065\(03\)00069-X](http://dx.doi.org/10.1016/S1474-7065(03)00069-X).
- Wigley, T., 1967. Non-steady flow through a porous medium and cave breathing. *J. Geophys. Res.* 72, 3199–3205.
- Yan, W.-M., Soong, C.-Y., 1995. Convective heat and mass transfer along an inclined heated plate with film evaporation. *Int. J. Heat Mass Transf.* 38, 1261–1269. [http://dx.doi.org/10.1016/0017-9310\(94\)00241-M](http://dx.doi.org/10.1016/0017-9310(94)00241-M).